LBL-15740 c.2
Preprint

Lawrence Berkeley Laboratory
UNIVERSITY OF CALIFORNIA

Materials & Molecular Research Division

Submitted to the Journal of Applied Physics

THE MICROSTRUCTURE AND CRITICAL CURRENT CHARACTERISTIC OF A BRONZE-PROCESSED MULTIFILAMENTARY NB_3SN SUPERCONDUCTING WIRE

I.W. Wu, D.R. Dietderich, J.T. Holthuis, M. Hong,
W.V. Hassenzahl, and J.W. Morris, Jr.

February 1983

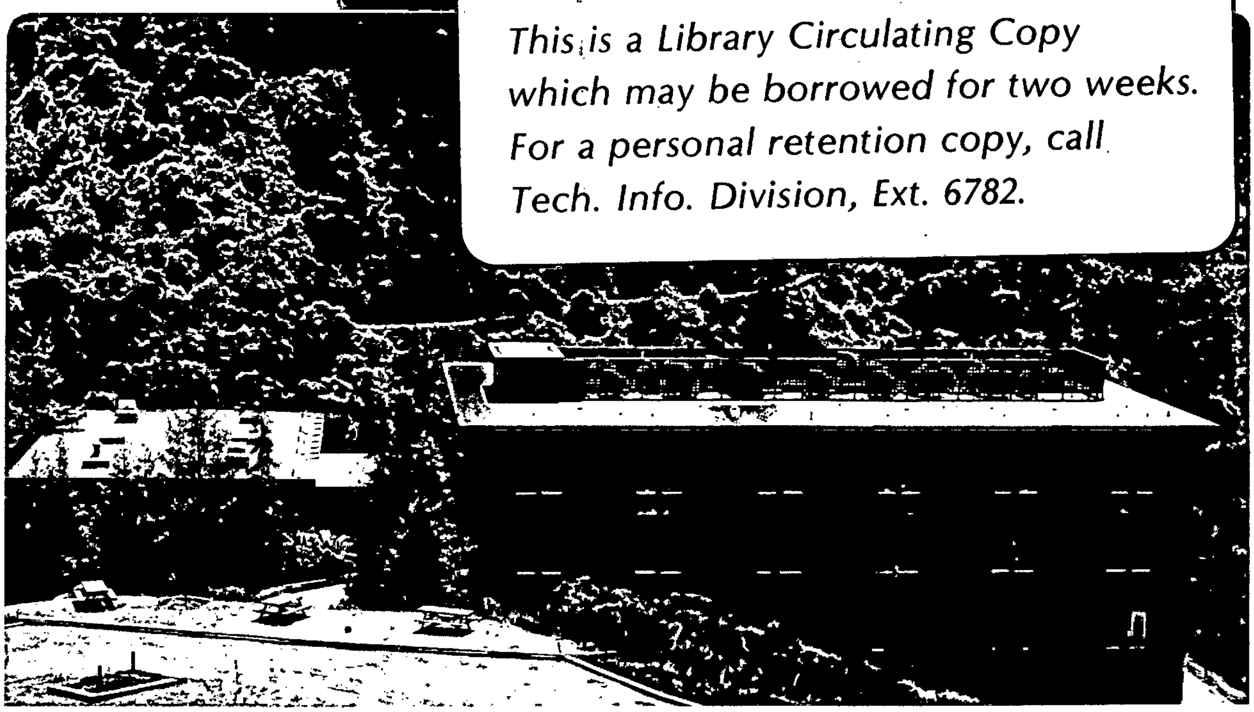

Prepared for the U.S. Department of Energy under Contract DE-AC03-76SF00098

DISCLAIMER

THE MICROSTRUCTURE AND CRITICAL CURRENT CHARACTERISTIC OF A BRONZE-PROCESSED MULTIFILAMENTARY NB_3SN SUPERCONDUCTING WIRE

I.W.Wu*, D.R.Dietderich*, J.T.Holthuis*, M.Hong†, W.V. Hassenzahl§ and J.W.Morris, Jr.*

Lawrence Berkeley Laboratory
University of California, Berkeley, Calif. 94720

ABSTRACT

The superconducting phase within a bronze-process, multifilamentary Nb_3Sn superconducting wire is formed by reaction at the interface between the Nb filaments and the bronze matrix. The maximum current that can be carried by the wire is known to depend on the time and temperature of the heat treatment as well as on the transverse magnetic field. In the work reported here a commercial Airco wire containing 2869 Nb filaments of 3-5 micron diameter in a matrix with a bronze/Nb ratio of 3 was given a variety of reaction heat treatments. The microstructure of the reacted layer was analyzed as a function of heat treatment, and found to be divisible into three concentric shells that are morphologically distinct. The central shell consists of fine, equiaxed grains. Its areal fraction, grain size and composition depend on the heat treatment, and appear to determine the critical current. The best combination of grain size and composition, and the highest critical current, is obtained with a intermediate reaction temperature (700-730°C). A further improvement in both microstructure and critical current is achieved by double-aging the wire so as to start the reaction at 700°C and finish it at 730°C. The relation between microstructure and heat treatment is interpreted in light of the apparent mechanisms of the reaction, which are revealed by high resolution analyses of the reacted layer. The relation between microstructure and properties is consistent with current understanding of the influence of grain size and stoichiometry on the behavior of type II superconductors.

*Materials and Molecular Research Division, Lawrence Berkeley Laboratory and Department of Materials Science and Mineral Engineering, University of California, Berkeley

†Bell Telephone Laboratories, Murray Hill, New Jersey

§Accelerator and Fusion Research Division, Lawrence Berkeley Laboratory

INTRODUCTION

The most common method for producing high field Nb_3Sn superconducting wires is the "internal bronze" process [1,2]. In this method niobium rods are inserted into a Cu-Sn bronze billet and drawn into a fine, multifilamentary wire. The wire is then heat treated to form the A15 Nb_3Sn superconducting phase through reaction at the niobium-bronze interface.

The maximum superconducting current, I_c, that can be carried by the reacted wire at a given temperature is determined by the wire diameter and the critical current density, J_c, within it. The critical current density is a function of the transverse magnetic field, H; the characteristic function, $J_c(H)$, depends on the area of the superconducting phase and on its microstructural state. The most important microstructural parameters are three: the composition and crystallographic order of the A15 crystal, the grain size, and the state of strain. The composition and order of the crystal determine its inherent superconducting properties [3-5]. The grain size controls the density of the most efficient flux line pinning sites [6-10] that prevent the loss of superconductivity at high current. The state of strain modifies the inherent superconducting properties, and is in part an internal strain that reflects the macrostructure of the superconducting composite [11].

The microstructural state of the superconducting wire cannot be controlled directly; it is determined indirectly by the starting geometry and the heat treatment. The relation between heat treatment and microstructure is not well understood, but must be identified and utilized if bronze-processed wires are to be engineered for maximum critical current. The present work was undertaken to characterize the microstructure of a typical wire with a fixed internal geometry, to establish the connection between the microstructure and the heat treatment the wire had received, and to correlate the microstructure and the superconducting properties. This work led into an effort to design heat treatments that would improve the microstructure so as to enhance the critical current. The success of the modified heat treatments has obvious engineering implications, but also gives credence to the qualitative relations between processing, microstructure and properties that emerge from the characterization studies.

Specific aspects of the work reported here have been published previously [12,13]. The present paper provides a more comprehensive presentation of the results and their implications. It should be noted that the research samples were commercial Airco wire with a fixed macrostructure and bronze/niobium ratio. The research concerned the nature and development of microstructure in this wire and its influence on the critical current characteristic in the relaxed condition; the influence of the elastic strain was not specifically considered. Okuda, et al. [14] have recently studied the consequences of varying filament size and the bronze/niobium ratio in similar multifilamentary superconducting wire. Their report includes a discussion of the influence of residual strain on the critical current in the relaxed condition. The maximum effect of the residual strain is small relative to that associated with significant changes in the microstructure.

EXPERIMENTAL PROCEDURE

A. Sample Geometry and Heat Treatment

The wire used in this investigation was manufactured by Airco Superconductors. It was a composite wire, 0.7mm in diameter, that contained an active core approximately 0.4mm in diameter. An etched section of the multifilamentary core is shown in Fig. 1. The core held 2869 niobium filaments grouped into sets of 19. The individual filaments were 3 to 5 microns in diameter. They were embedded in a Cu-13 wt.%Sn bronze matrix to give an overall bronze to niobium ratio of 3:1. The core was wrapped with a tantalum foil diffusion barrier approximately 30 microns thick. For thermal and electrical stabilization the wrapped core was encased in a pure copper shell, 0.15mm in thickness, that accounted for roughly two-thirds of the wire cross section.

Samples of the wire were heat treated after encapsulation in sealed quartz tubes that were back-filled with argon. They were reacted at temperatures in the range 650-800^{o}C for various times. The maximum reaction time at each temperature was that necessary to achieve an essentially complete conversion of the niobium filaments to Nb_3Sn.

B. Materials Characterization

The important materials parameters include the overall extent of the reaction at the Nb-bronze interface and the physical and chemical state of the superconducting layer formed.

The extent of reaction was determined by optical and scanning electron microscopic examination of etched cross sections of the heat treated wires. The A15 layer is easily distinguished from both the bronze matrix and the unreacted Nb core by its brittle appearance in broken wire sections and by its distinct etching behavior. A sample scanning electron micrograph of a polished and etched section is shown in Fig. 2.

The physical state of the reacted layer was studied by scanning electron microscopy (SEM) on broken and etched sections and by high resolution transmission electron microscopy (TEM) on thin sections. Samples for transmission electron microscopy began as longitudinal sections cut from the wire to reveal the multifilamentary material. The samples were ground to approximately 40 microns thickness, and then milled in an ion beam until perforated. They were examined in a Siemens 102 or JEOL-100C electron microscope at 100kV, using a 45^{o} double tilt goniometer stage to achieve the desired diffraction conditions. The principal object of these examinations was to determine the A15 grain size. The grain size could be roughly estimated from scanning electron micrographs of the broken wire surfaces. However, since only some of the grain boundaries appear in the fracture surface, the transmission electron microscopic analysis was essential to an accurate determination of the grain size. The values of the average grain size reported here were determined by the line intercept method on transmission electron micrographs. At least 100 grains were sampled for each datum point.

The chemical state of the reacted layer was studied with scanning transmission electron microscopy (STEM). The specimens employed were TEM foils prepared as described above. They were examined with a 100kV, 100A diameter electron probe in a Philips 400 electron microscope equipped with an energy dispersive x-ray spectrometer. The x-ray spectrum was analyzed quantitatively using a KEVEX 7000 microcomputer. The tin concentration within the reacted layer was determined from the x-ray spectra using a standardless approximation method [15] that has a 10-20% maximum error in the absolute value. A beryllium low-background stage with a 30° tilting axis was used to minimize spurious excitations. Residual niobium and 'in hole' configurations were examined to monitor the background shape and the peaks caused by inelastic scattering and spurious excitation. Nonuniformity in the specimen thickness is a further possible source of error; a specific investigation suggests that this error is less than 1 atom percent. The experimental arrangement and integrated count number were kept as nearly constant as possible to minimize systematic errors.

C. Superconducting Property Measurements

The superconducting properties that were determined included the overall critical current characteristic, $I_c(H)$ at 4.2K, and the transition temperature from the normal to the superconducting state, T_c. The transition temperature was measured inductively using a ring shaped sample of the wire with the copper stabilizer removed to minimize the shielding. The onset and finish temperatures of the superconducting transition were taken to be the temperatures that gave 10% and 90% of the total inductive signal, respectively. The critical current characteristic was measured by using a four-point probe technique on samples placed in transverse magnetic fields that ranged in intensity from 8 to 19.5 tesla. The reported value of the critical current is that which produced an 0.5 microvolt potential between voltage taps 5mm apart. All of the critical current measurements were done at the Francis Bitter National Magnet Laboratory.

The critical current density, $J_c(H)$, within the multifilamentary core of the wire was calculated from the critical current by dividing I_c by the cross-sectional area of the core, 0.14mm^2.

RESULTS AND DISCUSSION

Two sets of experiments were done. They differed in the type of heat treatment given the wires to form the A15 phase. Samples in the first set of wires were reacted at constant temperature in the range 650°C to 800°C. The superconducting properties of these wires were measured as a function of the reaction time and temperature and correlated with the microstructural state of the A15 layer. The results suggested that the microstructure of the A15 layer was far from optimal, even in the wires that had the highest critical current. The results were then used to guide the design of new, double-aging heat treatments to improve the microstructure and enhance the critical current. A second set of wires was prepared and tested to evaluate the new heat treatments.

A. Conventional Heat Treatments

1. Superconducting Properties

a. The critical current characteristic

Samples of multifilamentary wire were reacted at one of five temperatures, 650, 700, 730, 750 or 800^{o}C, for various times up to those necessary to achieve an essentially complete conversion of the Nb filaments to Nb_3Sn. The critical current of the wires was then measured at 4.2K in magnetic fields of 8-16 Tesla. Examples of the results are given in Table 1 and in Figures 3 and 4. The measured properties are in reasonable agreement with those found by Sanger, et al. [16] for similar wires.

The dependence of the critical current on the heat treatment time and temperature varied with the magnetic field. Figure 3, for example, shows the change in $J_c(H)$ with the time of heat treatment at 700^{o}C. The best low-field properties (8-12T) are achieved with the shorter aging times (2-6 days). Increasing the aging time to 8 days decreases the critical current at the lower fields even though it increases the areal fraction of A15 within the wire core (Table 2). At higher field (16T), on the other hand, J_c increases monotonically with the aging time.

The critical current characteristics of wires that had been reacted nearly to completion are plotted in Figure 4. The critical current is a strong function of reaction temperature only at the lowest (8-10T) and highest (15-16T) fields. Good low-field properties are associated with low reaction temperatures (650^{o}C) and short reaction times (730^{o}C/2 days). Good high-field properties seem to require a reaction temperature above 700^{o}C and a relatively long reaction time (Fig. 3).

b. The superconducting transition temperature

The superconducting transition temperature was measured for all heat treatment conditions. The results, which include an estimate of the width of the transition, are given in Table 1. The variation of T_c with aging time is plotted for three representative heat treatment temperatures in Figure 5. The data show that the critical temperature increases with aging time to an asymptote near 18K. The apparent width of the transition decreases with aging time.

2. The Microstructure of the Reacted Wire

a. The fraction of A15 phase

The micrographs presented in Figures 1 and 2 show that the filaments within the active core of the superconducting wire are somewhat irregular. The filaments differ slightly in shape, and a given filament has small variations in its cross section from point to point along its length. The variation in shape and diameter has the consequence that the reaction that forms the A15 layer is not strictly uniform.

Two parameters were used to measure the overall extent of the reaction: the mean thickness of the A15 layer on a filament, and the areal fraction of the A15 phase relative to the cross-sectional area of the unreacted filament. Both were determined from measurements on scanning electron micrographs of polished metallographic sections of the active core. The average thickness is plotted as a function of the reaction temperature and time in Figure 6. The areal fractions are given in Table 2. The data are in qualitative agreement with those reported previously [7,14,17,18].

As expected, the reaction rate increased dramatically with the aging temperature. An essentially complete reaction was defined as the conversion of more than 90% of the initial niobium to the A15 phase, and was achieved after 16 days at 650°C, 8 days at 700°C and 730°C, 2 days at 750°C, and 1 to 2 days at 800°C (Table 2).

b. The substructure of the A15 layer

i. The three-shell substructure. The microstructure of the A15 layer is clearly revealed only in transmission electron microscopic images. The analysis of a number of such images shows that the layer typically has the composite structure that is drawn schematically in Figure 7. The layer consists of three morphologically distinct shells. The innermost shell is made up of columnar grains that radiate out from the residual niobium core. A sample micrograph of this shell is given in Figure 8(a). The grains are roughly equiaxed in cross section and have a long axis approximately five times their diameter. The intermediate shell is made up of fine, equiaxed grains whose mean diameter (d) is approximately equal to the short, transverse diameter of the columnar grains in the inner shell. The outer shell, near the bronze matrix, is made up of large, irregular grains with diameters in the range 5-10d. A sample transmission electron micrograph is presented in Figure 8(b), and shows the fine-grained intermediate shell, the coarse outer shell, and the transition between them.

The general features of the microstructure are also apparent in scanning electron micrographs of broken filaments, such as those shown in Figure 9, but are not so clearly revealed. In particular, the fine-grained intermediate shell is rarely seen. Its absence is due to the fact that the SEM fractograph shows the fracture surface rather than the grain surface itself. Those grain boundaries that provide the easiest intergranular fracture path dominate the fracture surface. A detailed examination of the grain boundaries in the fine-grained layer (Figure 10) shows that these are most frequently low-angle grain boundaries that would not be expected to appear in intergranular fracture surfaces, and would not even be obvious in the transgranular segments of the fracture surface.

The overall morphology of the A15 layer is the same for all reaction times and temperatures studied. However, the microstructure of the layer is sensitive to the reaction conditions. The reaction temperature and time affect both the areal fractions of the three shells and the grain sizes within them.

ii. The areal fractions of shells within the layer. The thickness of each shell was measured as a function of reaction time and temperature from transmission electron micrographs. The areal cross sections were then estimated from the thickness of the shell and its inner or outer radius. The results are tabulated as a function of the heat treatment time and temperature in Table 2. The area fractions given in this table are relative to the initial cross-sectional area of the Nb filament.

The data presented in Table 2 reveal systematic changes with the reaction time and temperature. The fraction of columnar grains tends to decrease as the reaction temperature is raised, while the areal fraction of the coarse-grained shell increases with either the temperature or the reaction time. These two trends have the consequence that the highest fraction of fine-grained material is achieved by aging at intermediate temperature (700-730°C) for times that are sufficient to bring the reaction to about 90% completion. The maximum areal fraction of the fine-grained shell is plotted as a function of the reaction temperature in Figure 11.

iii. <u>The grain size within the fine-grained shell</u>. The mean grain size within the fine-grained shell increases monotonically with the reaction time and temperature as shown in Table 2. The mean grain size in the fine-grained shell of the almost fully-reacted wire increases exponentially with the reaction temperature, as shown in Figure 12.

The grain size data previously reported by Scanlan, et al. [6] and by Shaw [7] are also plotted in Figure 12. The data agree on the functional dependence of the grain size on the reaction temperature, but disagree on the magnitude of the grain size. Both Scanlan, et al. [6] and Livingston [8] used samples with much larger filament sizes than those employed here and found larger grains after a given heat treatment. Okuda, et al. [14] also report an increase in the grain size with the filament diameter. The filaments in the samples studied by Shaw [7] were comparable to ours, as were those in the wires examined by West and Rawlings [19] and by Schelb [20], but were in an uncertain state of reaction at the time the measurements were made. These authors report data that are roughly comparable to ours, but scatter significantly at the lower reaction temperatures.

iv. <u>The mechanism of reaction</u>. The essential features of the reactions that establish the three-shell structure of the A15 layer seem clear from the micrographs, although further work will be required to test them in detail. The key observations include the columnar grain structure at the Nb interface, the presence of arrays of dislocations within these grains, particularly near their outer boundaries (Figure 8(a)), the prevalence of low-angle grain boundaries in the fine-grained layer (Figure 10) and the frequency of dislocation arrays and pileups near the outer periphery of the columnar shell (Figure 13).

Both the morphology of the reacted layer and the absence of Kirkendall voids within the Nb core suggest that the reaction occurs by the diffusion of Sn to the Nb/Nb_3Sn interface. The reaction at the interface causes the growth of columnar grains that penetrate into the niobium. As the grains grow, they develop internal strains due to the volume and crystallographic changes associated with the transformation. The strains impel the formation and migration of dislocations that presumably originate from the columnar grain boundaries. The dislocation density builds up near the outer radius of the columnar region. The dislocations polygonize and effectively recrystallize the columnar grains into the fine-grained layer, in a reaction common to many crystalline materials. The fine-grained morphology is initially rather stable, but the continued reorganization of the grain boundary structure increases the mobility of the grain boundaries. The fine grains then coarsen to establish the coarse, outer shell.

In addition to agreeing with the microstructural observations of the reacted layer, this model is also consistent with the time and temperature dependence of the microstructure. At low temperature dislocations are relatively immobile. They should be generated in comparatively large numbers to relieve the strain, but their polygonization will be retarded. The columnar shell should hence be relatively thick, and eventually break up into very fine grains. At high temperature the dislocation mobility is higher, so the initial grain size in the fine-grained shell should be larger. But high temperature also increases the grain coarsening rate, so the coarse-grained shell should be thicker. It is therefore expected that the areal fraction of fine-grained material will pass through a maximum at an intermediate aging temperature while the grain size within the fine-grained shell increases monotonically with temperature. The microstructure should hence change with the reaction time and temperature very much as it is shown to change by the data given in Table 2.

c. The chemical state of the A15 layer

The important chemical properties of the A15 layer are its composition and state of order. Previous work [23,24] suggests that the crystalline order of Nb_3Sn is nearly ideal, irrespective of heat treatment. The composition profile of the layer was determined by STEM/EDXS analysis of the concentration of tin relative to that of niobium. While the analysis is subject to quantitative errors that were discussed above, the data that were obtained are mutually consistent and appear to be informative. Examples of the data are shown in Figure 14, which presents the measured Sn concentration profile as a function of reaction time at 700°C, and in Figure 15, which presents the concentration profile as a function of the reaction temperature for wires that have reached an essentially complete reaction. The data show that there is a gradient in the Sn concentration within the layer. The mean concentration gradient through the fine-grained shell is listed in Table 2 for all samples studied. Both the shape of the composition profile and its variation with time and temperature are of interest.

i. <u>The shape of the Sn concentration profile</u>. The Sn concentration decreases monotonically through the layer from an apparently Sn-rich composition at the bronze interface to a Sn-poor composition at the Nb interface. The compositions at the Nb interface are qualitatively consistent with the binary Nb-Sn phase diagram, in that they are lean in Sn by an amount that decreases with temperature (Figure 15). The phase relations at the Nb_3Sn-bronze interface are not known, but the measured composition at that interface is Sn-rich and becomes increasingly so as the temperature decreases. The composition profile through the layer is not smooth; it has a nearly flat central portion with steep concentration gradients near the two interfaces.

The shape of the concentration profile is consistent with current views on the mechanism of Sn diffusion. An idealized profile is shown in Figure 7 as an overlay on the microstructure of the reacted layer. It is widely accepted [17,21,22] that the principal Sn diffusion path through the A15 layer is along the Nb_3Sn grain boundaries. The Sn concentrations at the terminal points of the profile are fixed by the local equilibria between Nb and Nb_3Sn at the inner surface of the A15 layer and between Nb_3Sn and bronze at the outer surface. If the composition is different at the two interfaces, as it generally will be, then there must be a concentration gradient through the layer. But the much higher density of grain boundaries in the fine-grained central shell has the consequence that, if grain boundary diffusion dominates, the Sn composition can be homogenized within the intermediate shell at a much faster rate than it can diffuse into or out of it. The expected result is a flattening of the composition profile in the fine-grained layer with a concomitant steepening of the gradient near the two interfaces, just as is found experimentally.

ii. The change in the Sn profile with time and temperature. The Sn composition profile becomes flatter and more nearly stoichiometric as either the reaction time or the reaction temperature is increased (Figures 13 and 14; Table 2). There are three independent factors that lead to a flatter profile after long reaction times: homogenization within the fine-grained layer by grain boundary diffusion, the increase in the thickness of the fine-grained layer, and the depletion of Sn from the bronze, which decreases the Sn concentration at the outer boundary. Raising the reaction temperature also tends to flatten the profile, since it decreases the overall concentration change across the layer and increases the diffusivity. The temperature is a more potent variable than the time in this regard; the most constant, and, apparently, most nearly stoichiometric composition is obtained at the highest reaction temperature.

3. The Influence of Microstructure on Superconducting Properties

Two superconducting properties were measured: the superconducting transition temperature and, more importantly, the critical current characteristic. Both show the influence of the microstructure.

a. The critical current characteristic

The variation in the critical current characteristic, $J_c(H)$, with heat treatment has a reasonably straightforward and consistent explanation in terms of the composition and grain size of the A15 layer. The relative influences of the composition and the grain size should change with the magnetic field.

i. The critical current at low field. When the applied field is comparatively low, that is, below about 14T, virtually all of the A15 layer is superconducting and capable of carrying current. The critical current is then expected to vary roughly with the grain size. For samples with comparable grain size, the critical current should depend on the areal cross section of fine-grained material. It follows that the material reacted at the lower temperatures will have higher critical current, and that this current will be determined by some balance between the grain size in the fine-grained shell and its areal fraction. The smallest grain size results from the lowest reaction temperature (650^{o}C). The highest volume fraction of fine-grained material is obtained at a slightly higher reaction temperature (700-730^{o}C) and has a grain size that is only slightly larger. It is, therefore, not surprising that the best low-field properties are found after treatment at low to intermediate temperatures (Figure 4μ Table 1).

There is also an optimum reaction time for low-field properties. A specific example is given in Figure 3, where an increase in the reaction time at 700^{o}C from 2 to 6 to 8 days decreases the low-field critical current. The data presented in Table 2 offer a simple explanation for this phenomenon. Increasing the reaction time from 2 to 6 days increases the grain size within the fine-grained shell. However, there is a concommitant increase in the area of the shell. The net effect is a slight decrease in the low-field critical current. Extending the aging time to 8 days causes a substantial increase in grain size without a corresponding expansion in the area of the shell. The result is a substantial decrease in J_c.

ii. <u>The critical current at high field</u>. At higher field the critical current is sensitive to the composition of the layer as well as to its grain size. The upper critical field is known to be a strong function of composition. Only that subvolume of the reacted layer that is nearly stoichiometric should be able to support a high critical current density at fields of 16T or higher. The STEM/EDXS analyses suggest that there is at least some nearly stoichiometric material within the fine-grained shell at all reaction temperatures. But the fraction of nearly stoichiometric material depends on the magnitude of the Sn gradient, and the gradient decreases with both the reaction time and temperature (Table 2). It follows that the best high field conductors will be those that are treated for long times or at high temperatures, in agreement with the data shown in Figure 4. The best high field properties were obtained after long heat treatments at intermediate temperatures, for example, 700^{o}C for 8 days. The data presented in Table 2 show that these heat treatments result in a nearly uniform composition through an intermediate shell that retains a relatively small grain size.

The arguments presented here are qualitative. It should be possible to phrase them in a quantitative form. Research toward that end is now in progress. But a qualitative appreciation of the coupling between microstructure and critical current is sufficient to provide guidelines for process development. An apparently successful application of this understanding is described in the following section.

b. The superconducting transition temperature

Measurements of the superconducting transition temperature (Table 1) revealed two phenomena. As the reaction nears completion, the transition temperature increases monotonically toward 18K and the width of the transition decreases. Both phenomena are plausibly related to the state of the reacted layer.

at least a thin shell of nearly stoichiometric Nb_3Sn within the reacted layer. But the inductive T_c measures the transition temperature of a volume that is sufficient to expel the flux lines. Given the small values of the amplitude and frequency of the applied ripple field in a typical apparatus, the required volume is contained in a shell about 1 micron in thickness [25]. The particular subvolume of the layer that has the highest transition temperature is responsible for the experimental result. When the A15 layer is thinner than about 1 micron the inductive signal is not finished until virtually all the A15 phase is superconducting. Given the composition gradient through the layer, a thin layer will therefore show a broad transition with a center below 18K. When the layer is thick enough to have a region of nearly stoichiometric material that is of the order of one micron in thickness, the transition will be sharper and centered near 18K. The variation of the critical temperature and the transition width with heat treatment (Table 1) is hence reasonable in light of the variation of microstructure with heat treatment (Table 2).

The results presented here are consistent with those previously reported by Smathers and Larbalestier [25], by Evetts, et al. [26], and by Suenaga, et al. [27]. Okuda, et al. [14] have pointed out that small changes in T_c may also reflect the interplay between the strain, the variation of composition within the penetration depth, and the long range order parameter. It is clear that an exact analysis of the superconducting transition in a multifilamentary composite would require an elaborate theoretical treatment.

B. Double-Aging Treatments

1. Selection of a Double-Aging Treatment

Studies of the singly aged wires show that there are advantages to both low and high reaction temperatures. A low reaction temperature leads to a fine-grained microstructure and good low-field properties while a high reaction temperature leads to a better chemical distribution within the reacted layer and to an improved critical current at high fields. It is desirable to find an alternative heat treatment that combines the best features of both microstructures.

The simplest aging treatment that may combine the benefits of low and high temperature aging is a sequential, double-aging treatment in which a low temperature reaction is completed at higher temperature. In such a sequence the low temperature treatment is intended to establish a fine grain size while the high temperature treatment is included to improve the chemical distribution within the layer. The sequential treatment is at least superficially capable of improving the microstructure since chemical redistribution via grain boundary diffusion should occur more rapidly than grain growth. It is hence plausible that the fine grain size established at low temperature can be retained during a high temperature reaction that improves the stoichiometry of the layer.

Several combinations of double-aging time and temperature were used to test this hypothesis. These included: 650°C, 14-16 days + 730, 750 or 800°C, 0.5hr. to 2 days, and 700°C, 2-6 days + 730 or 750°C, 1-2 days. In each case the initial aging time was long enough to establish the general microstructure appropriate to the lower aging temperature.

2. The Double-Aged Microstructure

The A15 layer thickness is plotted as a function of the total reaction time of the double-aging treatments in Figure 16. The second, high temperature aging causes a rapid increase in the reaction rate and substantially shortens the time required to achieve an essentially complete reaction.

The distribution of grain size within the reacted layer is tabulated in Table 3 and illustrated in Figure 17. Those treatments that were finished at 730°C yielded a high areal fraction of fine-grained material with a small final grain size. The treatments that were finished at 750 or 800°C, on the other hand, produced a relatively thin intermediate shell with a rather coarse grain size. A 700°C initial aging was preferable to one at 650°C, primarily because of the greater thickness of the coarse-grained outer layer after the 650°C treatment.

Interestingly, as illustrated in Figure 17, the combined 700/730°C treatment produced a greater areal fraction of fine-grained material than was achieved by single aging at either temperature. It is not entirely clear why this beneficial effect happens. The reason may be that the relatively high defect density developed at the lower temperature (700°C) is rapidly polygonized at 730°C, but is partly lost if the reaction is continued to completion at 700°C because the long aging time permits some recovery. This explanation is supported by high resolution studies of the microstructure of the reacted layer in the double-aged condition. The overall morphology is similar to that of the reacted layer in the isothermally aged specimens, but the dislocation density appears to be greater both near the outer boundary of the columnar shell and within the fine-grained shell, as illustrated in Figure 18.

The Sn gradient through the reacted layer is tabulated in Table 3. Examples of the measured Sn profiles are plotted in Figure 19. The 700/730°C treatments appear to give a more nearly constant and stoichiometric distribution of Sn than either the single aging treatments or the double-aging treatments that are finished at 800°C. The reason for the small gradient is probably the combination of the small grain size and high areal fraction of the fine-grained layer, whose composition homogenizes at the higher reaction temperature. The 650/800°C treatment yields a very irregular Sn distribution. This is tentatively ascribed to the relatively short aging time at 800°C, which is not adequate to homogenize the layer.

The microstructural analyses show that the 700/730°C heat treatments establish an attractive combination of grain size, grain distribution, and chemical distribution within the reacted layer. The best of the treatments tested appears to be 700°C, 4 days + 730°C, 2 days.

3. The Superconducting Properties of Doubly-Aged Wires

The superconducting transition temperatures and critical currents of the doubly-aged wires are tabulated in Table 4. In Figure 20 the critical current characteristic of the best of the double-aged wires is compared to those of the two best of the isothermally aged group.

It is clear from this data that a proper double-aging leads to a substantial improvement in the critical current characteristic over the best attained with single aging treatments. The wire given the heat treatment 700°C, 4days + 730°C, 2 days has a critical current that is approximately fifty percent higher at all fields tested than the maximum measured after single aging. On the other hand, the double-aging treatments that were finished at 800°C did not improve the critical current, and caused an actual deterioration in the critical current at lower fields.

It also seems clear that the increase in J_c is due to the improvement in the microstructure of the reacted layer. The best double-aging treatments yield a reacted layer that contains a high areal fraction of fine-grained material with a reasonably constant Sn concentration. The microstructure combines the best features of low temperature and high temperature aging. The best double-aging treatments were finished at 730°C. Double-aging treatments that were finished at 800°C were ineffective because of the rapid grain growth at this temperature.

CONCLUSION

The research reported here appears to demonstrate a simple and necessary connection between the heat treatment and the critical current characteristic of bronze-process multifilamentary Nb_3Sn superconducting wire. The connection is made through the microstructure of the superconducting phase. Both the physical and the chemical states of the A15 layer that forms around the Nb filament are relevant to the superconducting properties. The most striking physical feature of the reacted layer is its three-shell composite structure. The critical current density is apparently determined by the areal fraction, grain size and composition of the central, fine-grained shell.

The areal fraction and the microstructure of the fine-grained shell depend on heat treatment. Isothermal reaction at lower temperatures (650°C) creates a fine grain size, but yields a low fraction of fine-grained material that has a relatively poor composition. Isothermal reaction at high temperature (800°C) establishes a good composition profile, but yields a large grain size and low critical current. Isothermal aging at intermediate temperature (700-730°C) gives the best combination of microstructural features and the highest critical current. Both the microstructure and the critical current can be improved further by double-aging treatments that start the reaction at 700°C and finish it at 730°C. This treatment produces a large areal fraction of fine-grained material with a nearly constant composition, and enhances the critical current density by approximately 50%.

The microstructure can be plausibly related to the heat treatment through the apparent mechanisms of the reaction forming the A15 phase. These mechanisms are inferred from the results of high resolution studies of the development of the microstructure. The critical current varies with the microstructure, and specifically with grain size and stoichiometry, as current understanding suggests it should.

ACKNOWLEDGMENTS

The authors are grateful to J. Glazer, Materials and Molecular Research Division, Lawrence Berkeley Laboratory, for assistance in the preparation of the manuscript, and to L. Rubin and his associates at the National Magnet Laboratory for advice and assistance in the conduct of the critical current measurements. The critical current measurements were performed at the Francis Bitter National Magnet Laboratory, supported by the National Science Foundation. This work was supported by the Director, Office of Energy Research, Office of Basic Energy Sciences, Materials Sciences Division, and by the Director, Division of High Energy Physics, U. S. Department of Energy under Contract No. DE-AC03-76SF00098.

REFERENCES

1. A. R. Kaufmann and J. J. Pickett, **Bull. Am. Phys. Soc.**, 15, 833, 1970.

2. E. W. Howlett, U.S. Pat. 3,728,165 (filed 10/19/1970); Great Britain Pat. 52,623/69 (filed 10/17/69).

3. B. E. Jacobson, R. H. Hammond, T. H. Geballe and J. R. Salem, **J. Less Common Metals**, 62, 59, 1978.

4. T. P. Orlando, J. A. Alexander, S. J. Bending, J. Kwo, S. J. Poon, R. H. Hammond, M. R. Beasley, E. J. McNiff and S. Foner, **IEEE Trans. Mag.**, MAG-17, 368, 1981.

5. D. B. Smathers and D. C. Larbalestier, in **Filamentary A15 Superconductors**, M. Suenaga and A. F. Clark (eds.), Plenum Press, New York (1980) p. 143.

6. R. M. Scanlan, W. A. Fietz and E. F. Koch, **J. Appl. Phys.**, 46, 2244, 1975.

7. B. J. Shaw, **J. Appl. Phys.**, 47, 2143, 1976.

8. J. D. Livingston, **Phys. Stat. Sol. (a)**, 44, 295, 1977.

9. G. Zerweck, **J. Low Temp. Phys.**, 42, 1, 1981.

10. E. J. Kramer, **Adv. Cryo. Eng.**, 28, 307, 1982.

11. J. W. Ekin, **Cryogenics**, 20, 611, 1980.

12. M. Hong, I. W. Wu, J. W. Morris, Jr., W. Gilbert, W. V. Hassenzahl and C. Taylor, **Adv. Cryo. Eng.**, 28, 435, 1982.

13. I. W. Wu, W. V. Hassenzahl and J. W. Morris, Jr., **Proceedings, International Cryogenic Materials Conference**, Kobe, Japan, 1982, K. Tachikawa and A. Clark, eds., Butterworths, London, p. 388.

14. S. Okuda, M. Suenaga and R. L. Sabatini, **J. Appl. Phys.**, 54, 289, 1983.

15. J. I. Goldstein, in Introduction to Analytical Electron Microscopy, J. J. Hren, J. I. Goldstein and D. C. Joy (eds.) Plenum Press, New York (1979), p. 83.

16. P. A. Sanger, E. Adam, E. Ioriatti and S. Richards, **IEEE Trans. Mag., MAG-27**, 666, 1981.

17. K. Togano, T. Asano and K. Tachikawa, **J. Less Common Metals**, 68, 15, 1979.

18. M. Suenaga, K. Aihara, K. Kaiho and T. S. Luhman, **Adv. Cryo. Eng.**, 26, 442, 1980.

19. A. W. West and R. Rawlings, **J. Mat. Sci.**, 12, 1862, 1977.

20. W. Schelb, **J. Mat. Sci.**, 16, 2575, 1981.

21. H. H. Farrell, G. H. Gilmar and M. Suenaga, **J. Appl. Phys.**, 45, 4025, 1974.

22. A. A. Bochvar, V. S. Sergeev, V. G. Kuznetsova, A. D. Nikulin, E. A. Klepatskaya and M. A. Fomishkin, **Metallovedenie i Termicheskaya Obrabotka Metallov.**, 12, 44, 1980.

23. R. Flukiger, **Adv. Cryo. Eng.**, 28, 399, 1982.

24. J. L. Standenmann, **Solid State Phys.**, 23, 121, 1977; 26, 461, 1978.

25. D. B. Smathers and D. C. Larbalestier, **Adv. Cryo. Eng.**, 28, 415, 1982.

26. J. E. Evetts, J. R. Cave, R. E. Somekh, J. P. Stanton, and A. M. Campbell, **IEEE Trans. Mag.**, MAG-17, 360, 1981.

27. M. Suenaga, in Superconductor Materials Science, S. Foner and B. B. Schwartz, eds., Plenum Press, New York, 1981, p. 201.

FIGURE CAPTIONS

1. A scanning electron micrograph of the cross section of a typical multifilamentary Nb_3Sn wire sample.

2. A scanning electron micrograph showing the reacted A15 layer around the filaments. The sample was heat treated at 700°C for 6 days.

3. The critical current characteristic, $J_c(H)$, for samples reacted at 700°C for 2, 6, and 8 days.

4. The critical current characteristic, $J_c(H)$, for samples that were isothermally aged to essentially complete reaction at 650, 700, 730 and 800°C.

5. The inductive superconducting transition temperature, T_c, as a function of aging time for samples that were isothermally reacted at 650, 730 and 800°C.

6. The average A15 layer thickness as a function of aging time for samples that were reacted isothermally at 650, 700, 730 and 800°C.

7. Schematic representation of the overall morphology of a reacted A15 layer (a) with an overlay showing an idealized Sn composition profile through the layer (b).

8. Transmission electron micrographs of the three distinct shells in the reacted layer of a sample that was aged at 730°C for 2 days: (a) columnar grains near the Nb core, (b) grains within the fine-grained and coarse-grained shells.

9. Scanning electron micrographs showing the fracture surfaces of broken filaments that had been reacted at (a) 650°C for 16 days and (b) 700°C for 6 days. Note that the fine, equiaxed grains in the layer center are not obvious on the fracture surface.

10. A transmission electron micrograph of a sample aged at 750°C for 2 days, showing the columnar and fine-grained shells. Note that the grain boundaries in the fine-grained shell are primarily low angle boundaries.

11. The areal fraction of the fine-grained shell, relative to the original cross section of the Nb filament, as a function of the aging temperature for wires that were aged to essentially complete reaction.

12. The average grain size within the fine-grained shell as a function of the aging temperature for samples that were isothermally aged to essentially complete reaction. The data of Scanlan et al. [6] and Shaw [7] are included for comparison.

13. A high resolution transmission electron micrograph showing dislocation pileups in the columnar grains. The sample was isothermally aged at 700°C for 6 days.

14. The Sn concentration profile across the reacted layer, as determined by STEM/EDXS analysis for samples aged isothermally at 700°C for 2 and 8 days.

15. The Sn concentration profile across the reacted layer, as determined by STEM/EDXS analysis for samples reacted isothermally to near completion at temperatures in the range 650 to 800°C.

16. The average thickness of the A15 layer as a function of aging time. The solid lines are for isothermal aging at 650 and 700°C. The dotted lines continue the curves for the temperature and time of double aging.

17. The areal fraction of fine equiaxed grains in the reacted layers of the doubly aged specimens, relative to the original cross section of the Nb filament. The comparable data for singly aged specimens is reproduced from Figure 11.

18. A transmission electron micrograph of the fine-grained shell within a sample that was doubly aged at 700°C for 6 days plus 730°C for 1 day. Examples of dislocation pileups and low angle grain boundaries are indicated by arrows.

19. The Sn concentration profiles, as determined by STEM/EDXS analysis, for three doubly aged specimens.

20. The critical current characteristic, $J_c(H)$, for a sample aged at 700°C/4 days + 730°C/2 days. $J_c(H)$ is compared to those attained by the best isothermal treatments: 700°C/6 days and 730°C/2 days.

TABLE 1. The results of superconducting properties measurements: J_c data at 10, 14 and 15 tesla and inductive T_c onset and transition width for various isothermal treated specimens.

AGING CONDITION	OVERALL J_c, 10^3 AMP/CM^2 10T	14T	15T	T_c(K) ONSET (Δ T_c)
650°C/4D	33.3	8.9	6.4	17.5 (0.6)
8D	37.9	11.0	8.0	17.7 (0.3)
16D	40.5	15.7	10.8	17.9 (<0.1)
700°C/2D	46.0	15.7	10.4	17.5 (0.5)
6D	44.3	17.1	12.2	17.7 (0.2)
8D	36.3	17.9	13.8	17.9 (0.1)
730°C/4hr	34.3	9.0	6.1	17.4 (0.4)
1D	38.7	11.1	11.8	17.9 (0.1)
2D	46.7	16.4	13.1	17.9 (<0.1)
8D	44.0	14.5	12.7	18.0 (<0.1)
750°C/2D	44.6	16.3	12.7	17.9 (0.4)
800°C/12hr	18.6	8.1	6.2	17.9 (0.3)
2D	31.4	15.7	12.7	18.0 (<0.1)

TABLE 2. The results of microstructural analyses of the A15 layer for isothermal treated samples.

Aging Condition	Volume Fraction				Grain Size, d (Å)	Sn Gradient At.% Sn/μm
	Columnar Grain	Equiaxed Grain	Coarsened Grain	Total		
650°C/4D	.31	.32	—	.63	530	—
8D	.25	.33	.29	.87	600	—
16D	.27	.34	.32	.93	630	4.7
700°C/2D	.13	.37	.23	.76	640	8.5
4D	.17	.43	.26	.86	720	—
6D	.17	.46	.28	.91	740	5.4
8D	.18	.47	.29	.94	770	5.2
730°C/20min	.11	.15	.07	.33	540	—
1hr	.14	.17	.08	.39	590	—
1D	.15	.37	.29	.81	690	—
2D	.13	.42	.33	.88	720	5.3
8D	.10	.39	.46	.95	800	5.1
750°C/2D	.14	.34	.46	.93	840	—
800°C/4hr	.16	28	.31	.75	—	—
12hr	.22	.24	.44	.90	1090	6.2
2D	.14	.31	.52	.97	1190	2.1

TABLE 3. The results of microstructural analyses of the A15 layer for several doubly-aged specimens.

Aging Condition	Volume Fraction				Grain Size, d (Å)	Sn Gradient At.% Sn/μm
	Columnar Grain	Equiaxed Grain	Coarsened Grain	Total Grain		
650°C/14D + 730°C/2D	.16	.40	.42	.98	650	—
650°C/16D + 800°C/4hr	.22	.28	.46	.96	930	10.8
700°C/2D + 730°C/2D	.15	.48	.31	.94	730	2.0
700°C/4D + 730°C/2D	.11	.58	.29	.98	760	2.3
700°C./6D + 730°C/1D	.12	.56	.30	.98	770	2.5
700°C/2D + 750°C/2D	.12	.43	.43	.98	830	2.6

TABLE 4. The results of superconducting properties measurements (J_c and T_c) for several doubly-aged samples.

AGING CONDITION	OVERALL J_c, 10^3 AMP/CM^2 10T	14T	15T	T_c(K) ONSET (ΔT_c)
650°C/14D + 730°C/2D	56.5	17.8	12.5	17.6 (0.3)
650°C/14D + 750°C/2D	48.5	16.0	11.8	17.8 (0.2)
650°C/16D + 800°C/0.5hr	45.8	14.8	10.0	17.8 (0.2)
700°C/2D + 730°C/2D	57.1	22.9	17.9	17.6 (0.3)
700°C/4D + 730°C/2D	61.4	25.1	20.7	18.0 (0.5)
700°C/6D + 730°C/1D	58.2	23.5	17.5	17.8 (<0.1)
700°C/2D + 750°C/2D	55.5	21.2	15.3	17.9 (0.2)

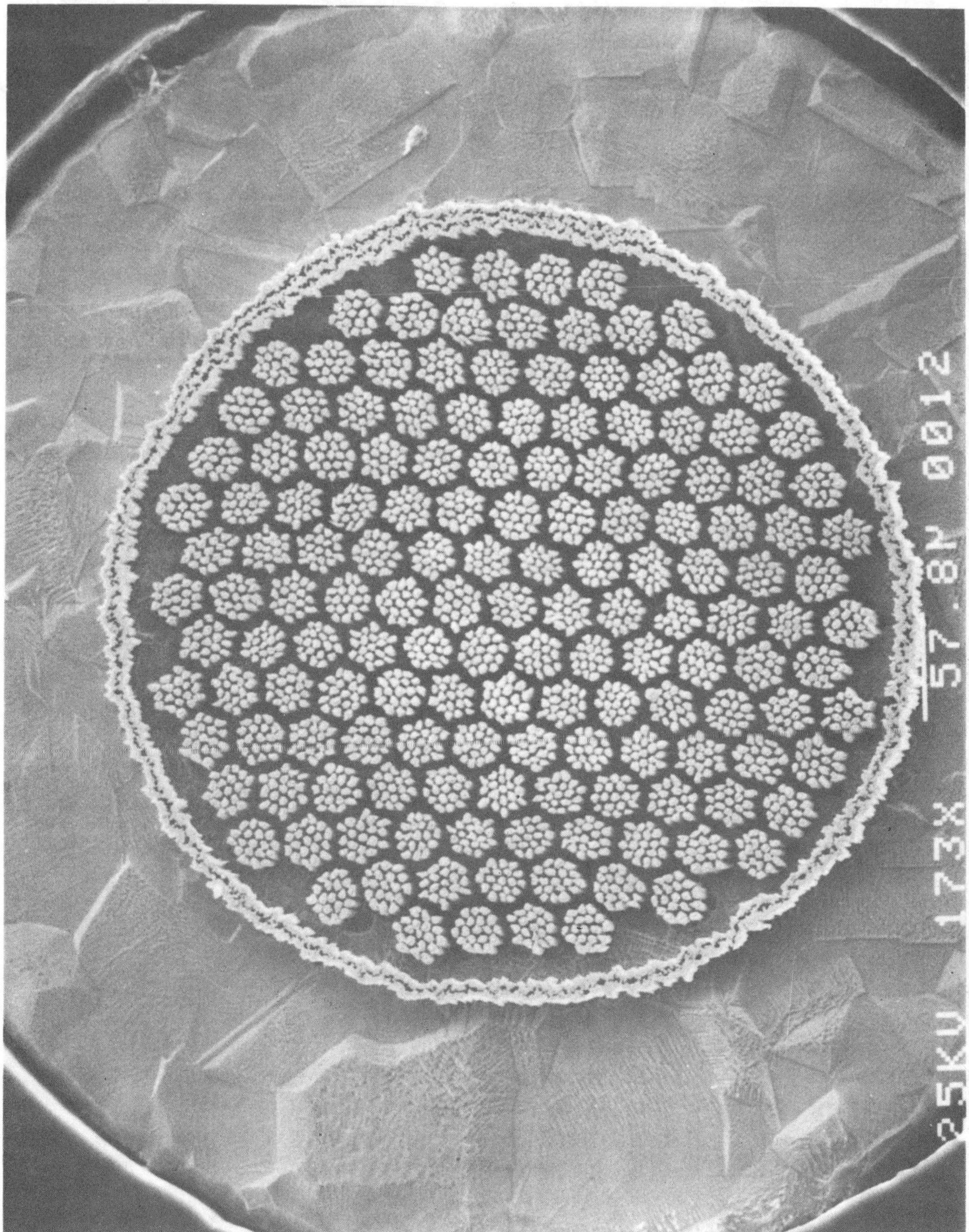

XBB 831-546

Figure 1

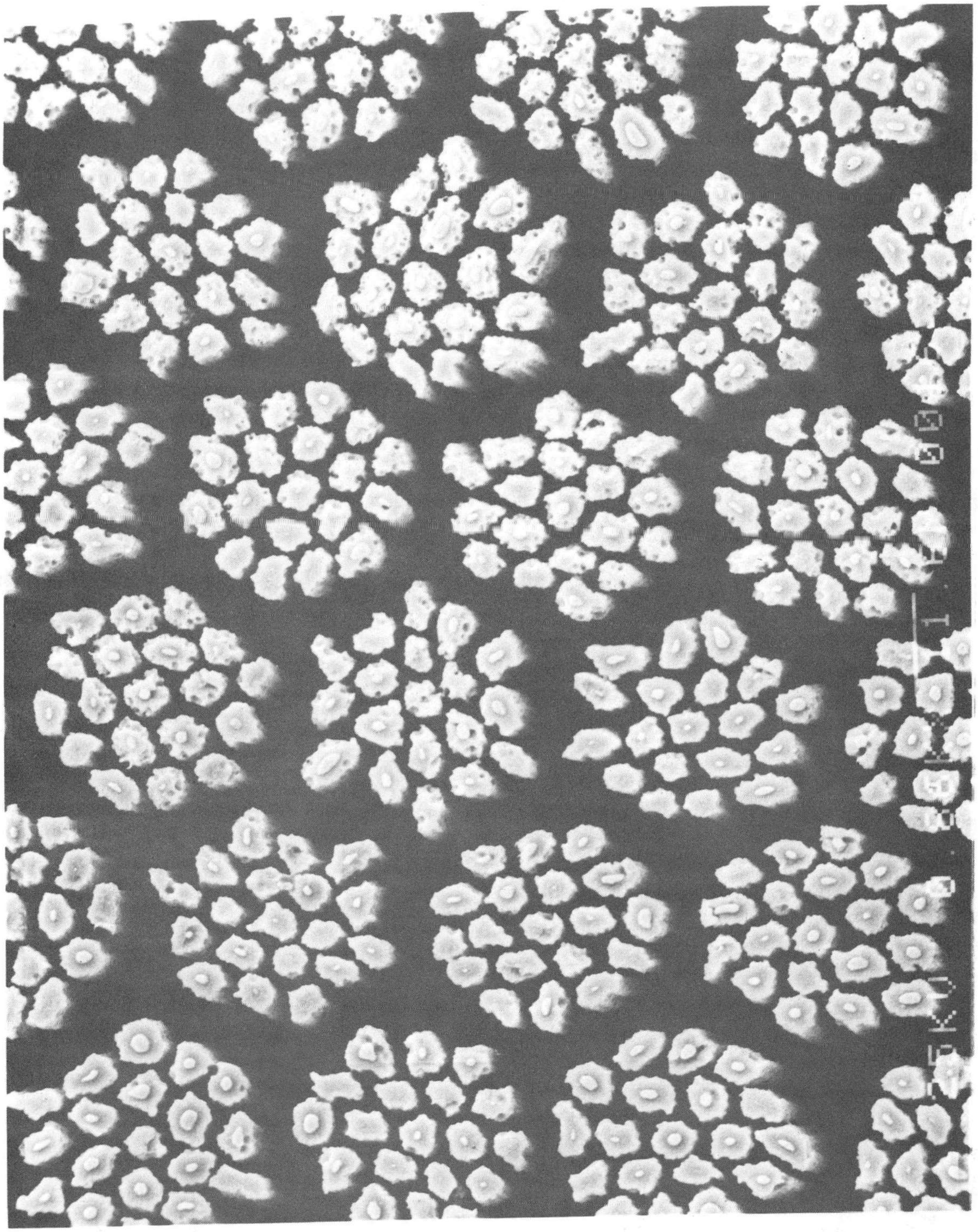

XBB 831-957

Figure 2

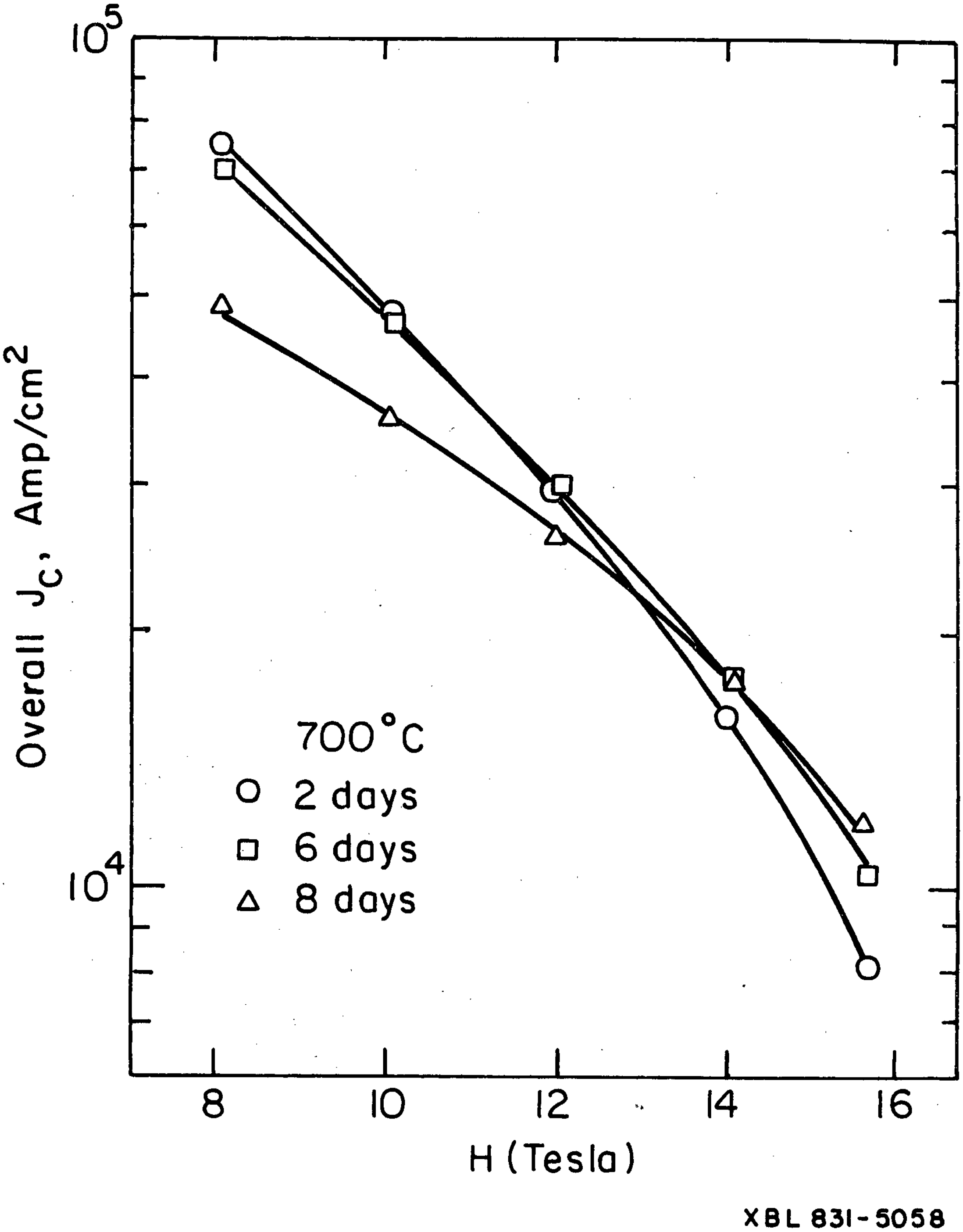
10^5
10^4
Overall J_c, Amp/cm^2
700°C
2 days
6 days
8 days
8
10
12
14
16
H (Tesla)
XBL 831-5058

Figure 3

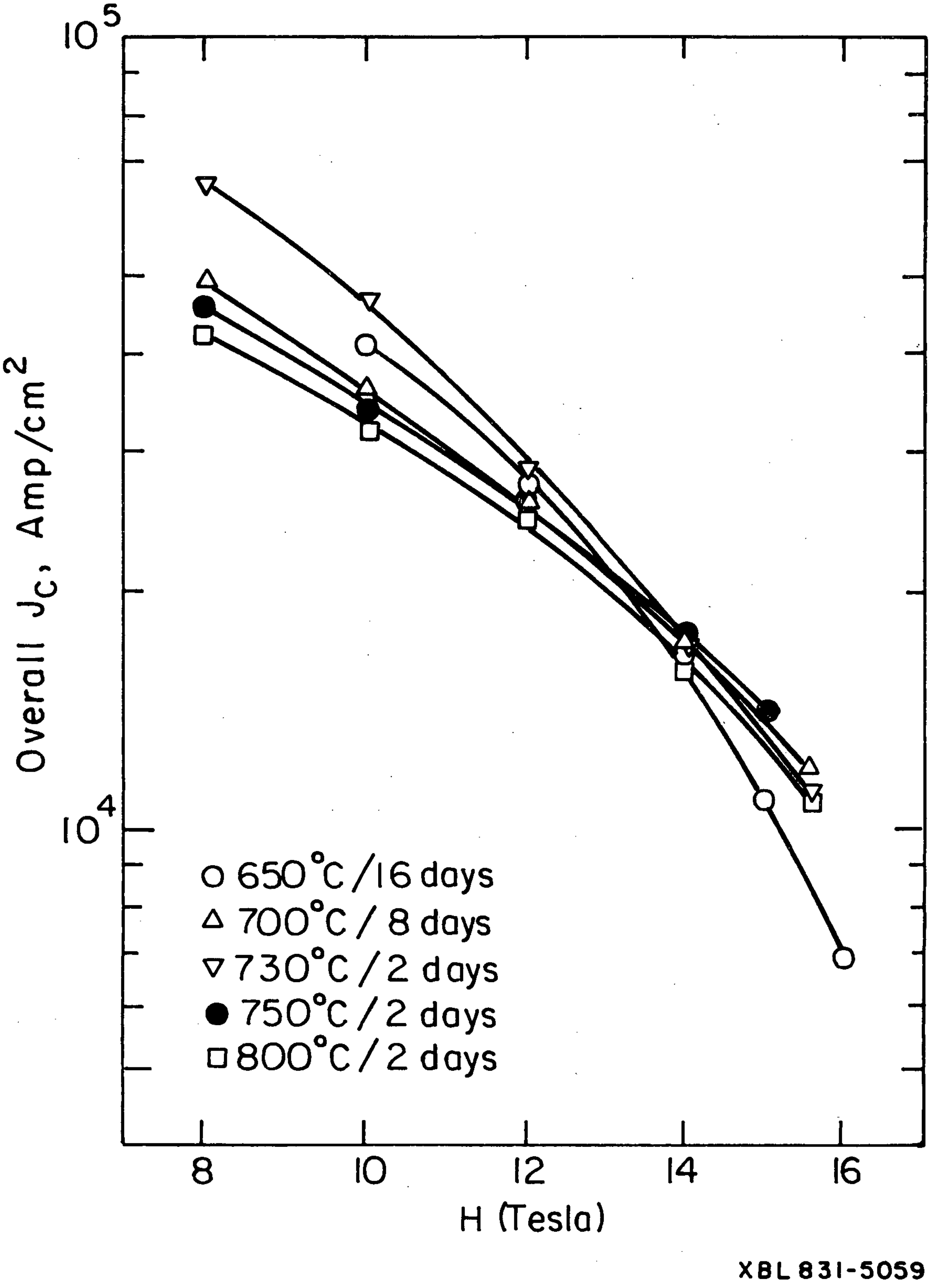

10^5
10^4
Overall J_c, Amp/cm^2
8
10
12
14
16
H (Tesla)
○ 650°C /16 days
△ 700°C / 8 days
▽ 730°C / 2 days
● 750°C / 2 days
□ 800°C / 2 days
XBL 831-5059

Figure 4

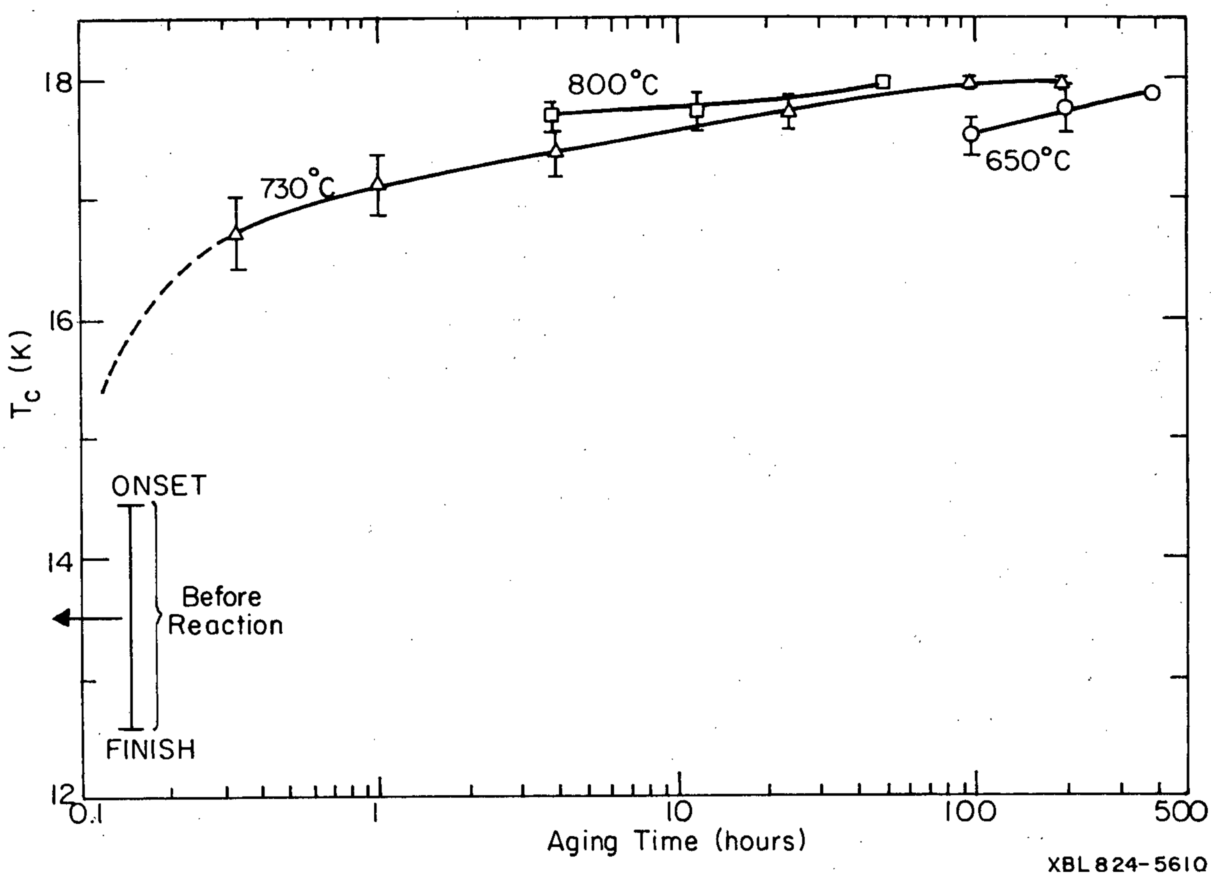

18
16
14
12
T_c (K)
800°C
730°C
650°C
ONSET
Before
Reaction
FINISH
0.1
1
10
100
500
Aging Time (hours)
XBL 824-5610

Figure 5

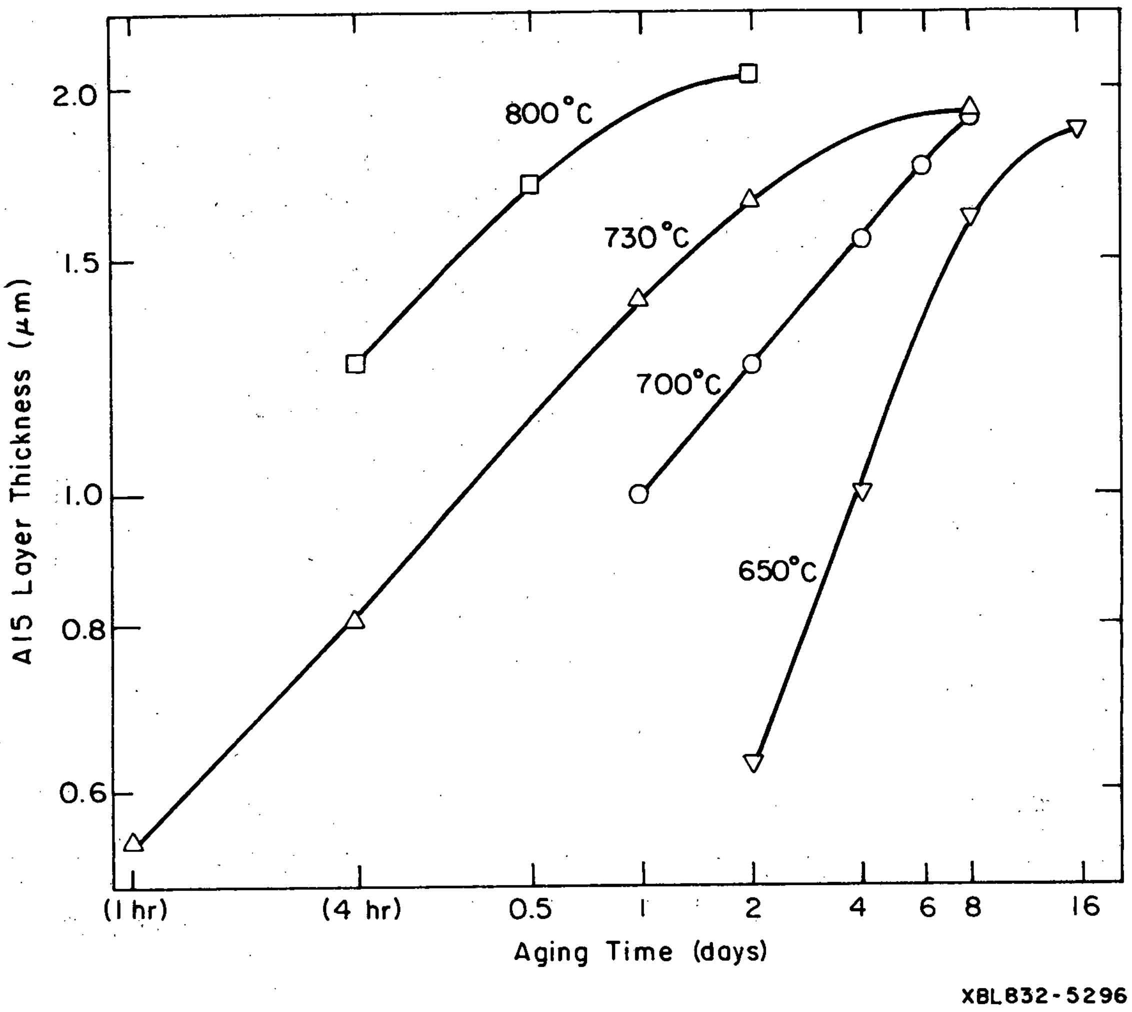

800°C
730°C
700°C
650°C
2.0
1.5
1.0
0.8
0.6
A15 Layer Thickness (μm)
(1 hr)
(4 hr)
0.5
1
2
4
6
8
16
Aging Time (days)
XBL832-5296

Figure 6

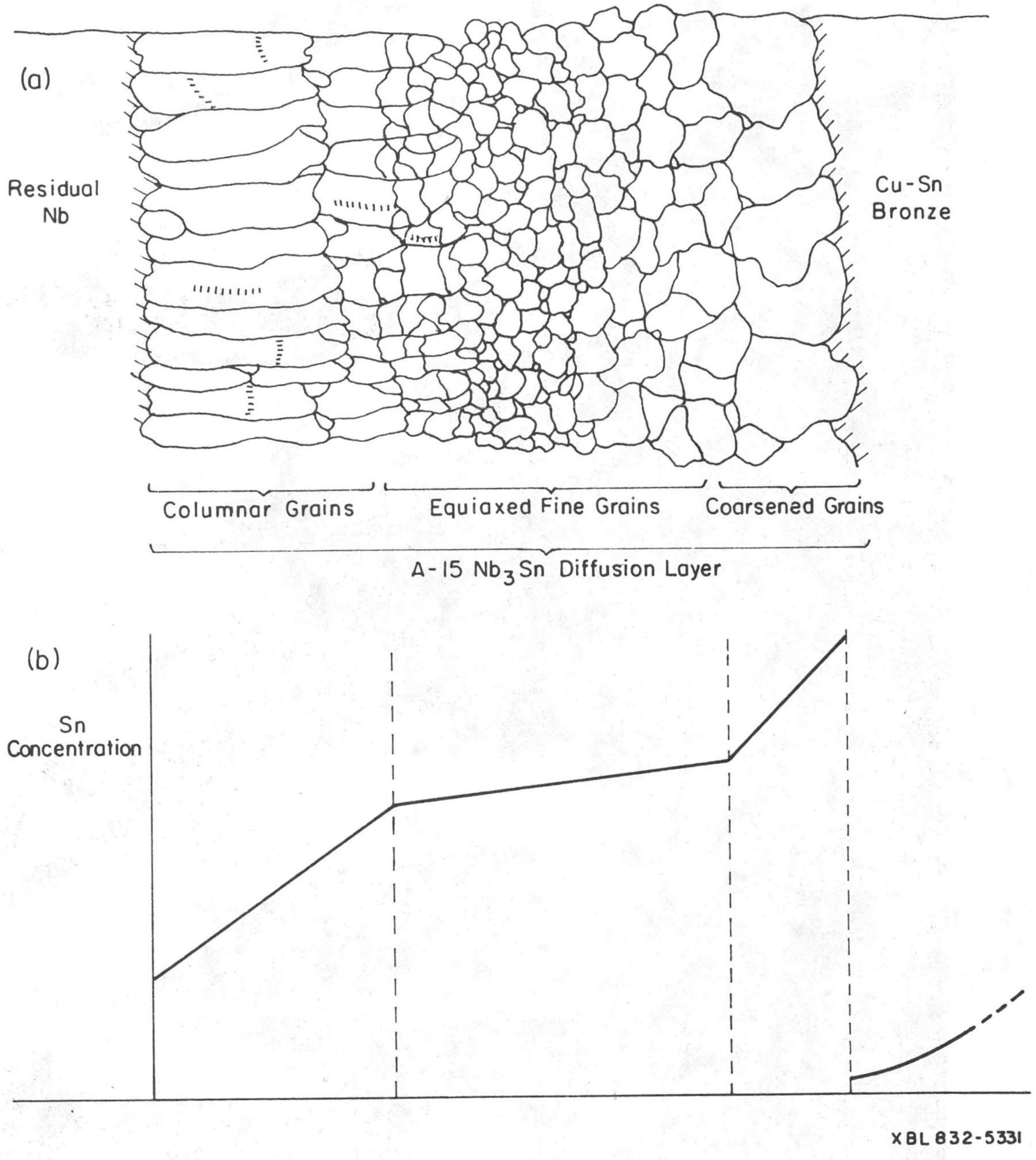
(a)
Residual Nb
Cu-Sn Bronze
Columnar Grains
Equiaxed Fine Grains
Coarsened Grains
A-15 Nb_3Sn Diffusion Layer
(b)
Sn Concentration
XBL 832-5331

Figure 7

XBB 818-7133

Figure 8 (a)

XBB 818-7138

Figure 8 (b)

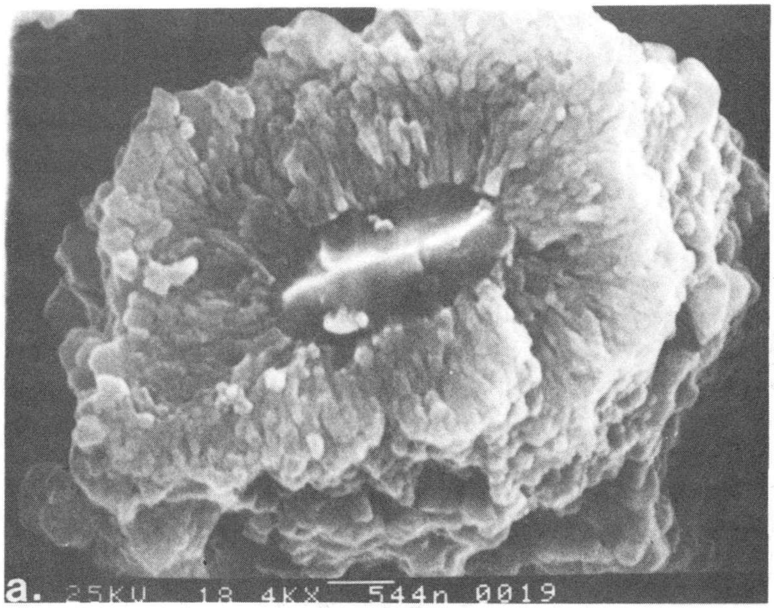

650°C/16DAYS

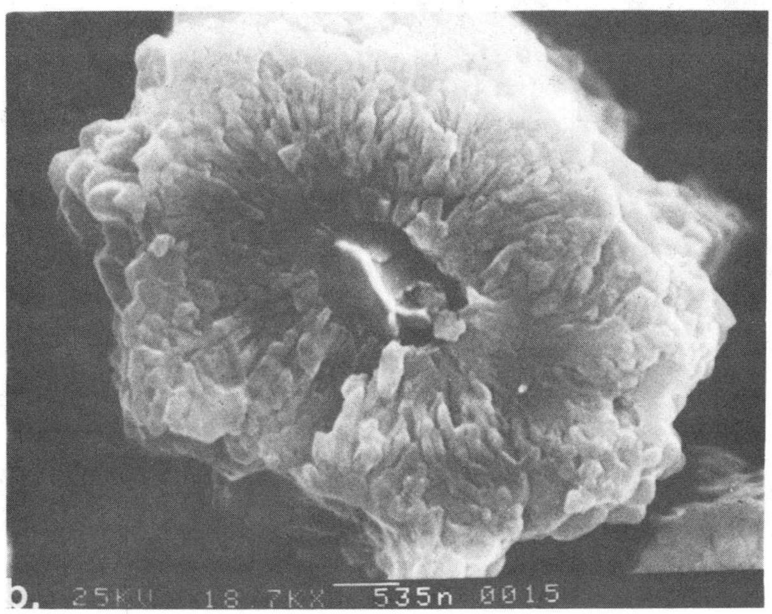

700°C/6DAYS

XBB 831-226A

Figure 9

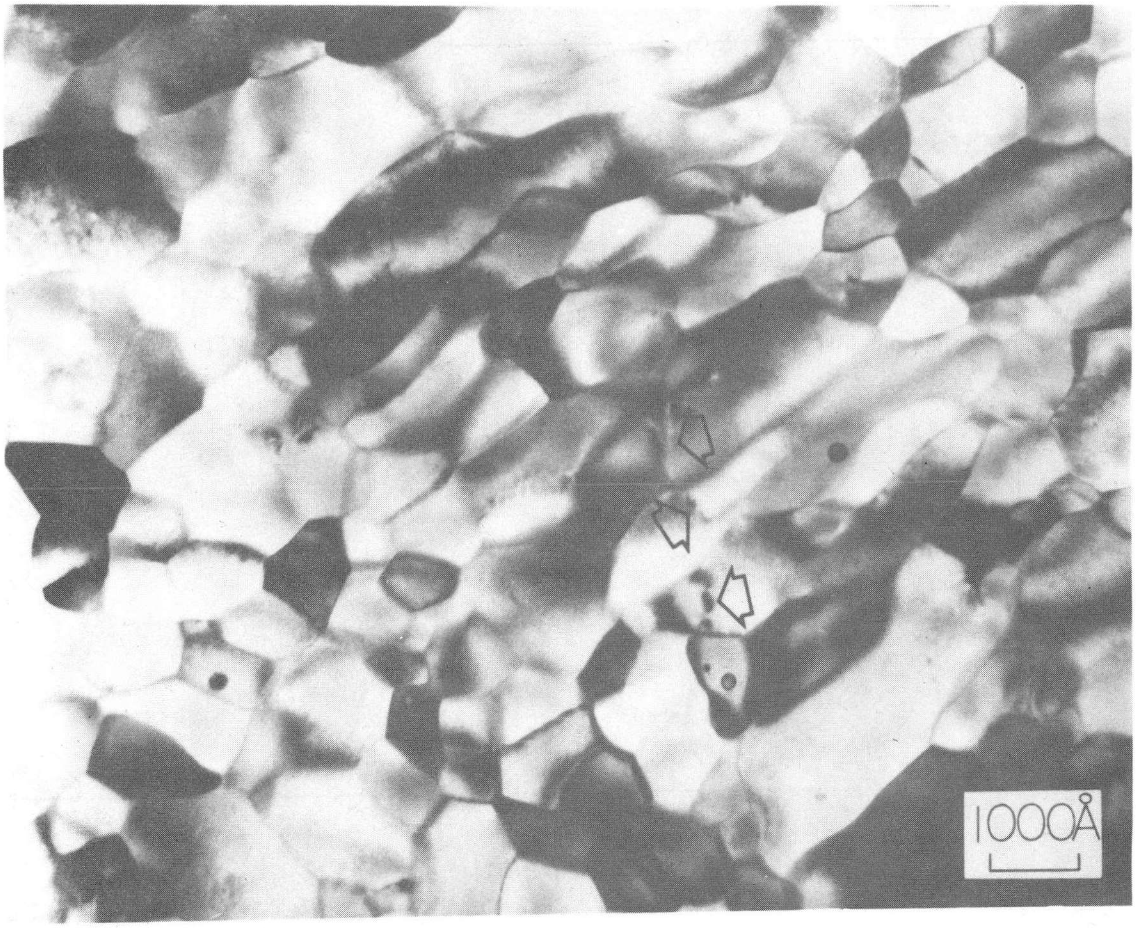

XBB 824-4087

Figure 10

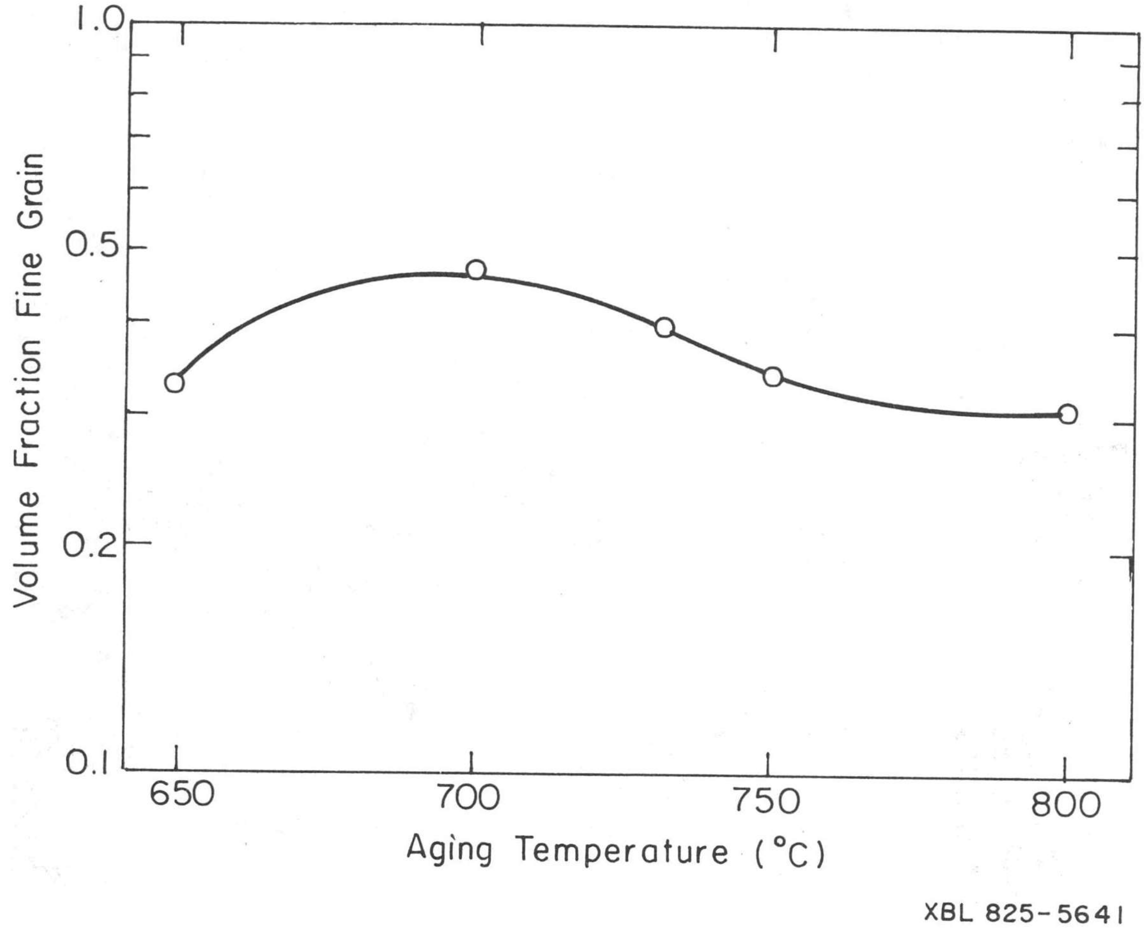
1.0
0.5
0.2
0.1
Volume Fraction Fine Grain
650
700
750
800
Aging Temperature (°C)
XBL 825-5641

Figure 11

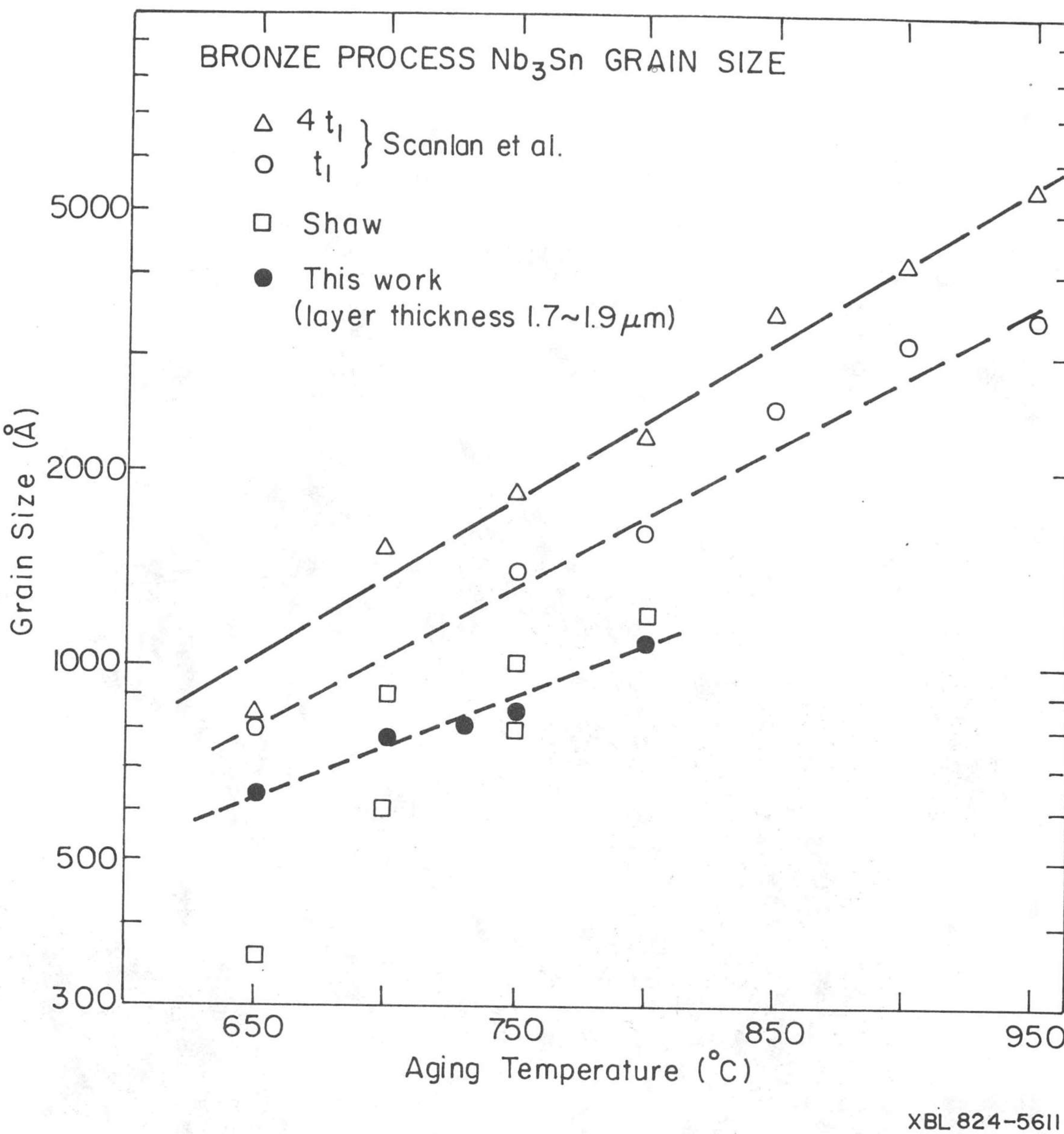
BRONZE PROCESS Nb_3Sn GRAIN SIZE
△ $4t_1$
○ t_1
Scanlan et al.
□ Shaw
● This work
(layer thickness 1.7~1.9μm)
Grain Size (Å)
5000
2000
1000
500
300
650
750
850
950
Aging Temperature (°C)
XBL 824-5611

Figure 12

XBB 825-4151

Figure 13

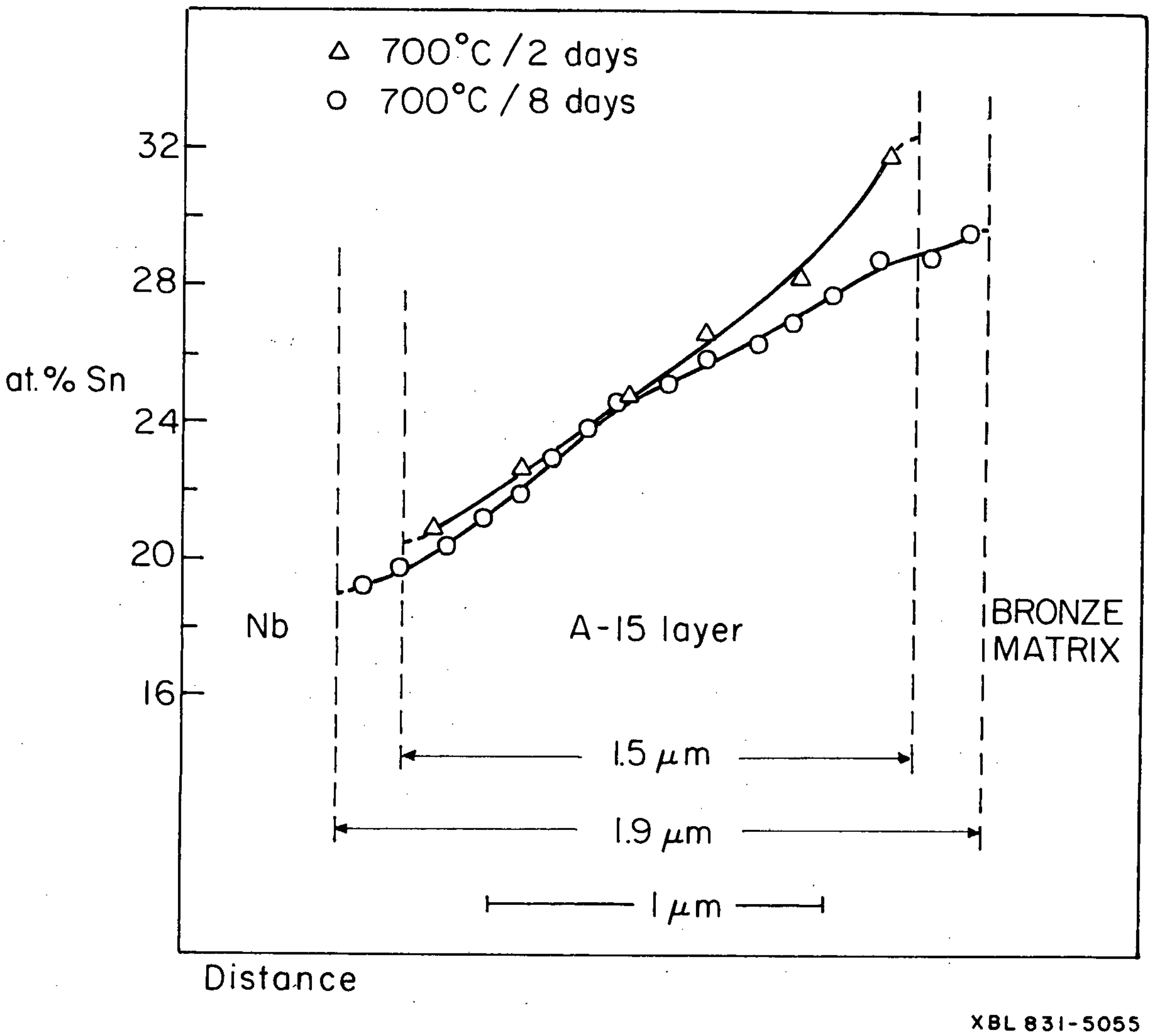
△ 700°C / 2 days
○ 700°C / 8 days
32
28
24
20
16
at.% Sn
Nb
A-15 layer
BRONZE
MATRIX
1.5 μm
1.9 μm
1 μm
Distance
XBL 831-5055

Figure 14

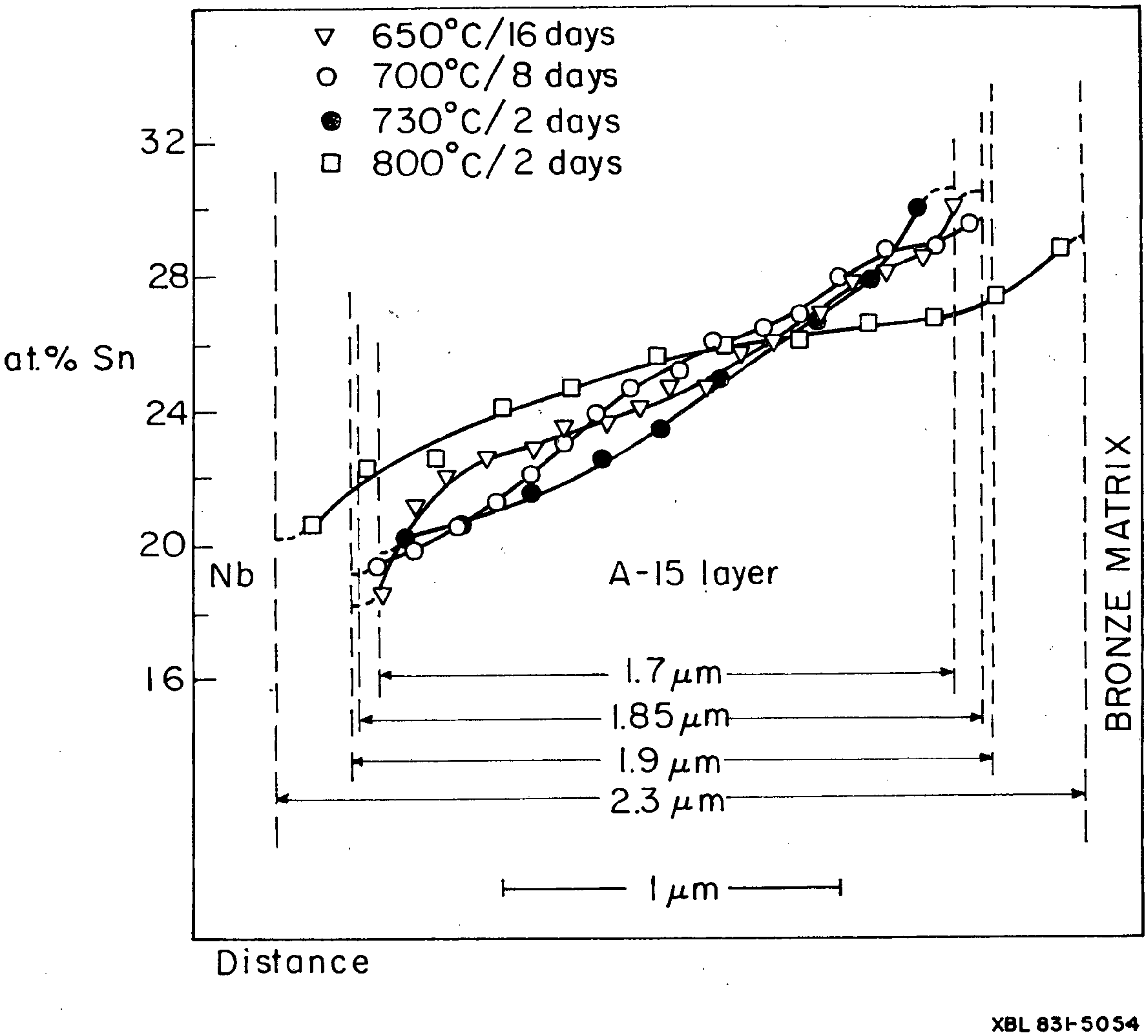

▽ 650°C/16 days
○ 700°C/8 days
● 730°C/2 days
□ 800°C/2 days
32
28
24
20
16
at.% Sn
Nb
A-15 layer
BRONZE MATRIX
1.7 μm
1.85 μm
1.9 μm
2.3 μm
1 μm
Distance
XBL 831-5054

Figure 15

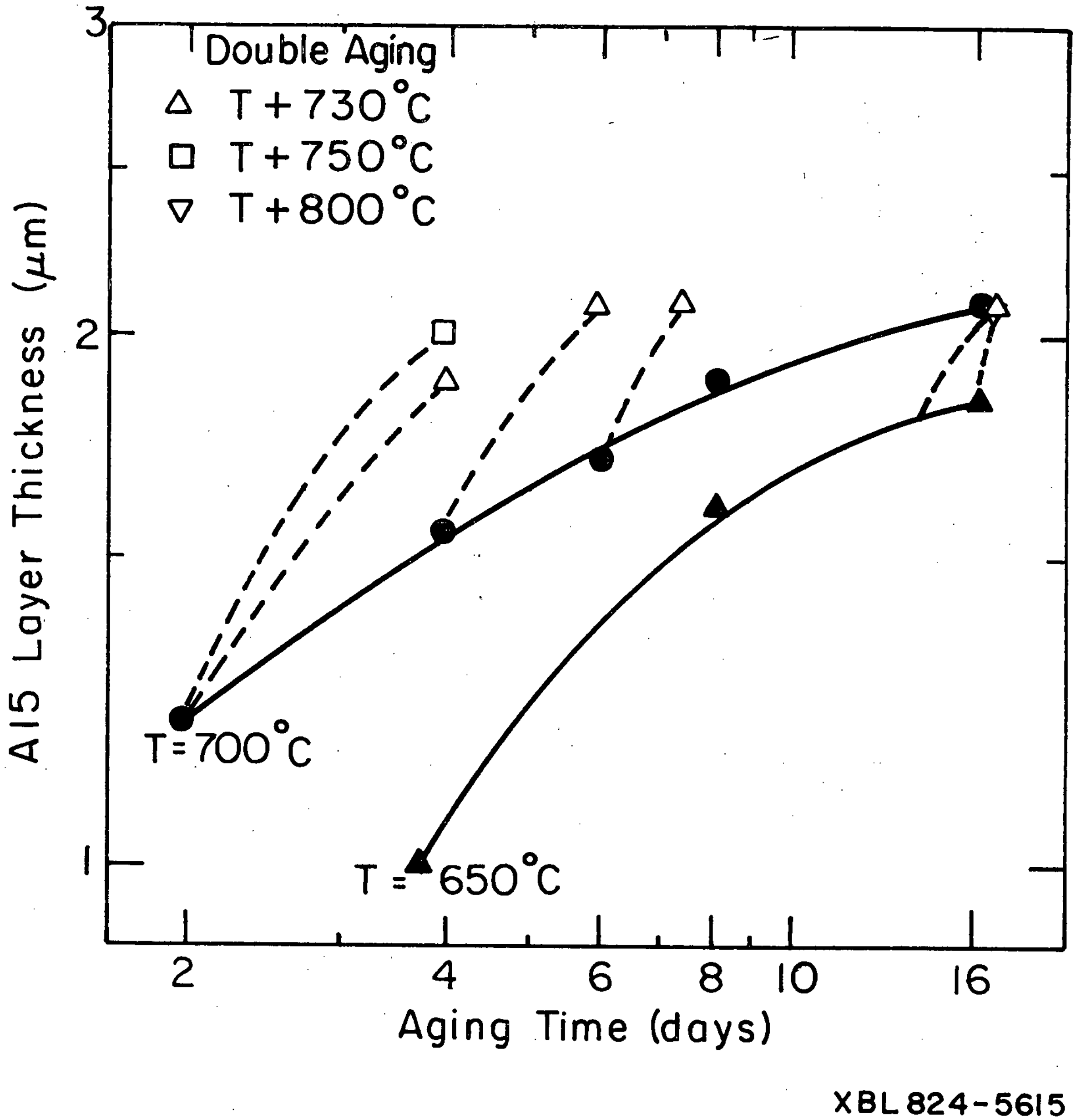
Double Aging
T + 730°C
T + 750°C
T + 800°C
A15 Layer Thickness (μm)
3
2
1
T=700°C
T = 650°C
2
4
6
8
10
16
Aging Time (days)
XBL 824-5615

Figure 16

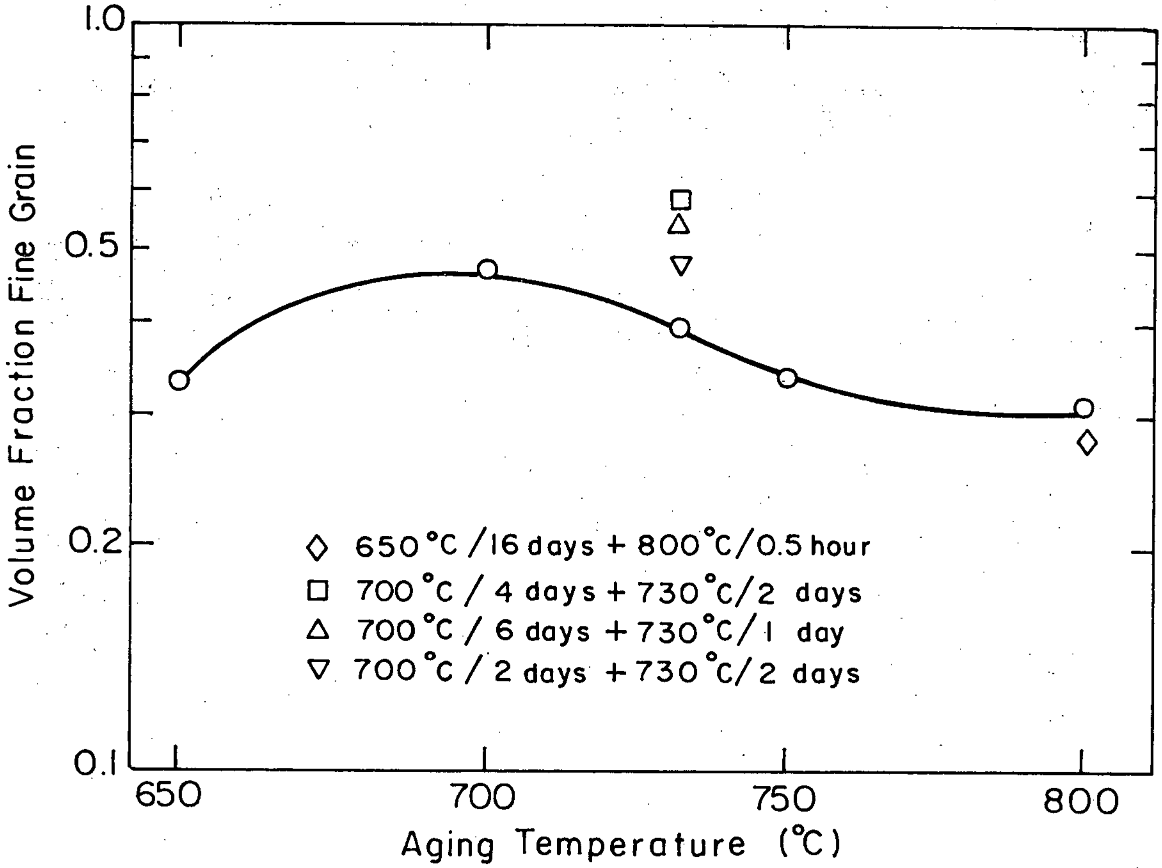

XBL 825-5642

Figure 17

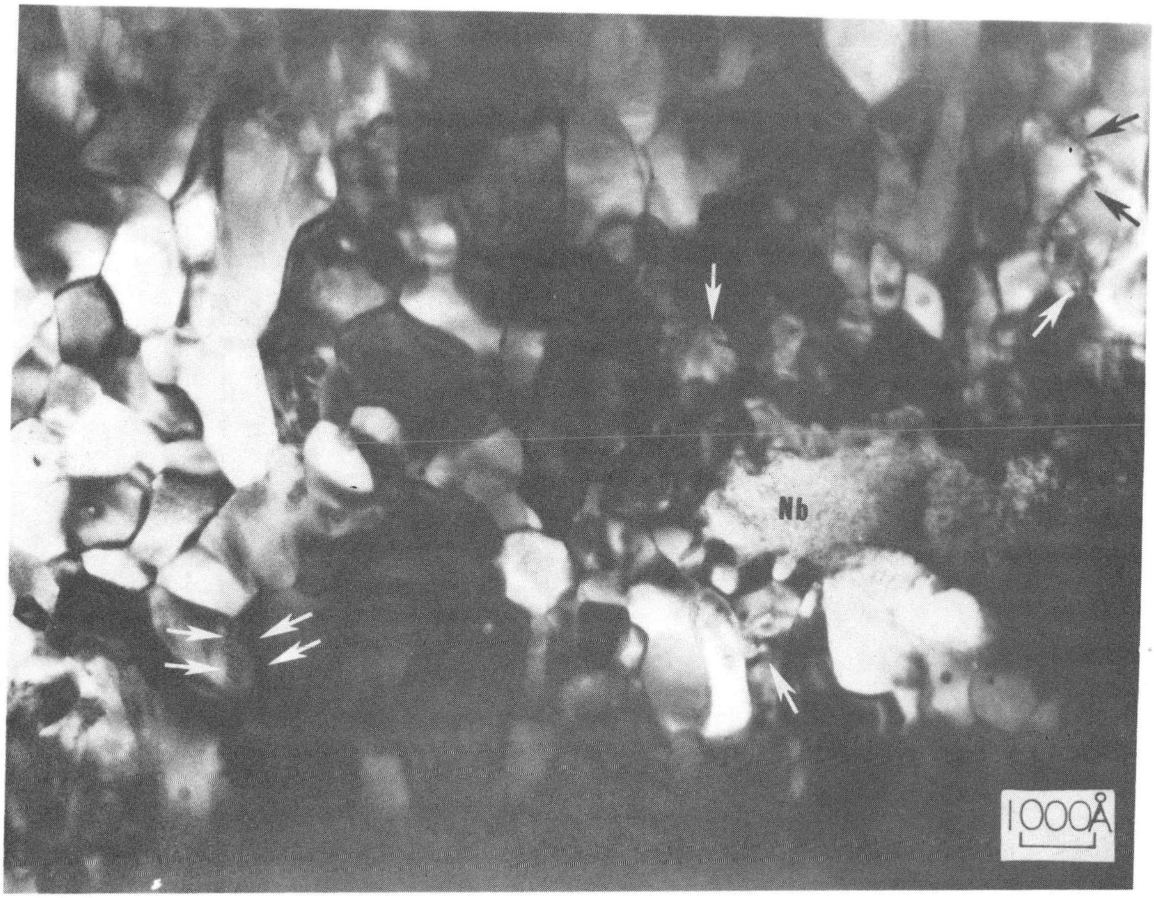

XBB 822-1157

Figure 18

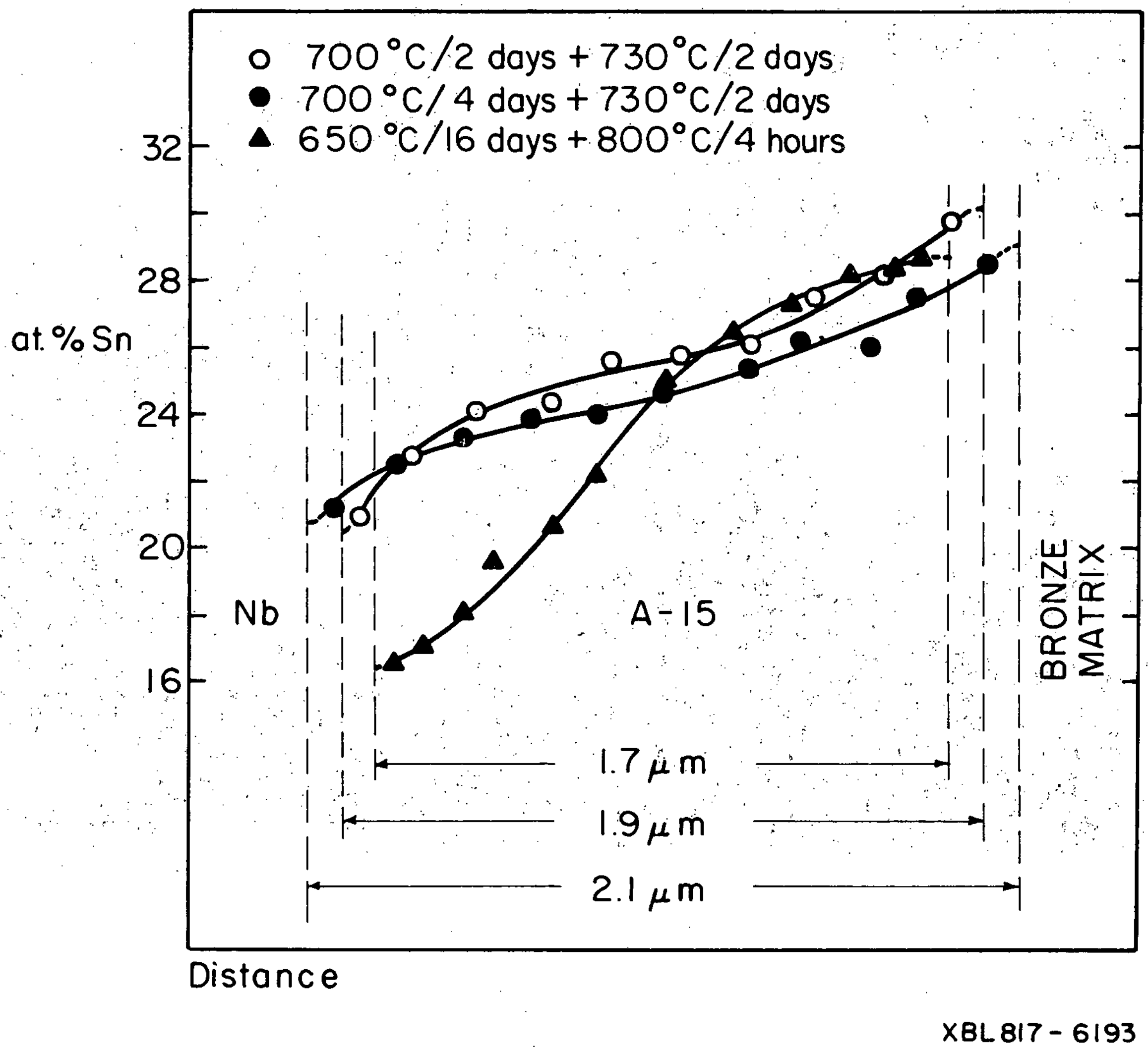
○ 700°C/2 days + 730°C/2 days
● 700°C/4 days + 730°C/2 days
▲ 650°C/16 days + 800°C/4 hours
32
28
at.% Sn
24
20
16
Nb
A-15
BRONZE MATRIX
1.7 μm
1.9 μm
2.1 μm
Distance
XBL817-6193

Figure 19

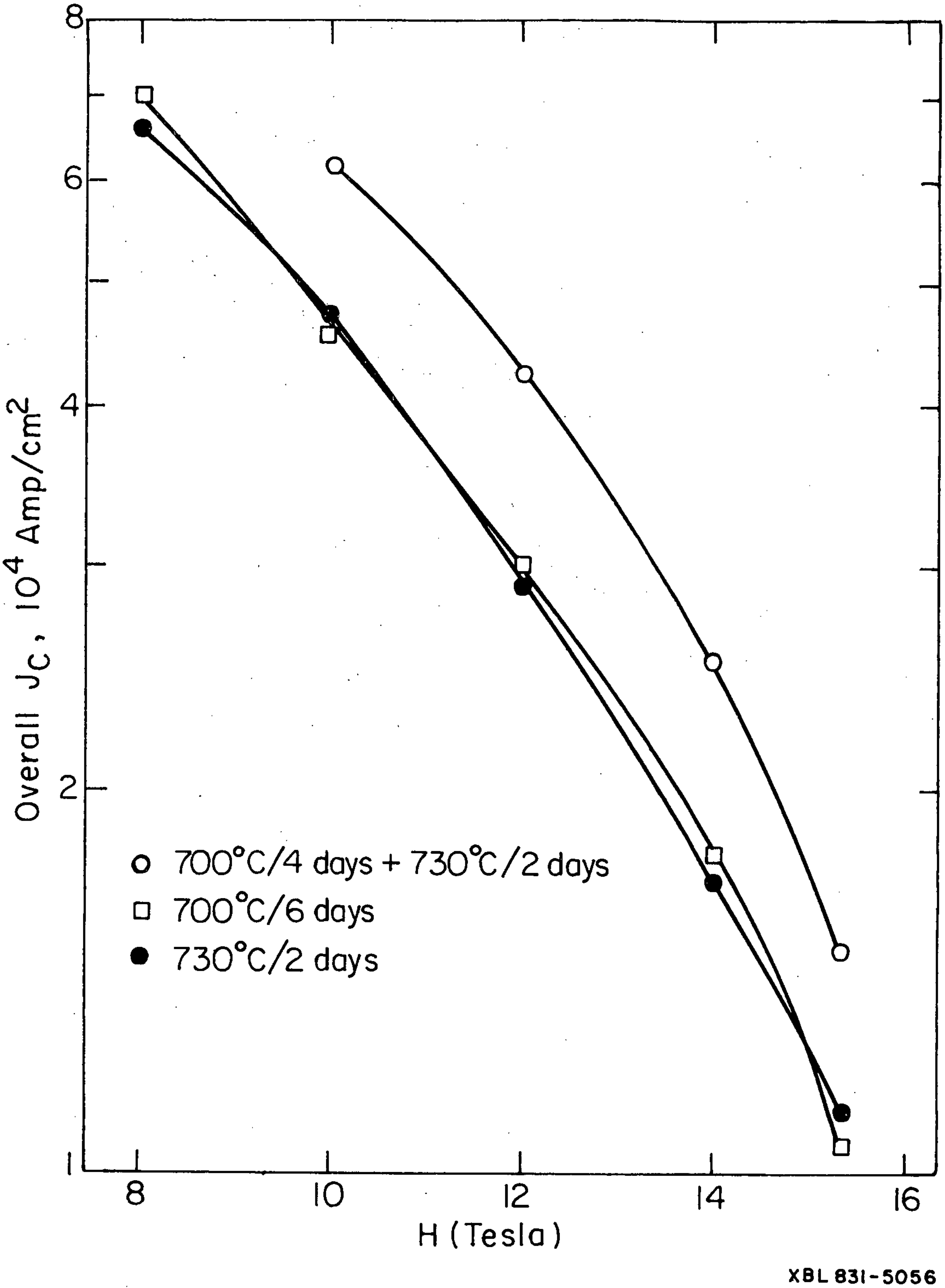
8
6
4
2
1
Overall J_C, 10^4 Amp/cm^2
○ 700°C/4 days + 730°C/2 days
□ 700°C/6 days
● 730°C/2 days
8
10
12
14
16
H (Tesla)
XBL 831-5056

Figure 20

TECHNICAL INFORMATION DEPARTMENT
LAWRENCE BERKELEY LABORATORY
UNIVERSITY OF CALIFORNIA
BERKELEY, CALIFORNIA 94720